COPY 6
RM E54I29

NACA RM E54I29

NACA

RESEARCH MEMORANDUM

EXPERIMENTAL INVESTIGATION OF A 0.4 HUB-TIP DIAMETER RATIO AXIAL-FLOW COMPRESSOR INLET STAGE AT TRANSONIC INLET RELATIVE MACH NUMBERS

II - STAGE AND BLADE-ELEMENT PERFORMANCE

By John C. Montgomery and Frederick W. Glaser

Lewis Flight Propulsion Laboratory
Cleveland, Ohio

NATIONAL ADVISORY COMMITTEE
FOR AERONAUTICS

WASHINGTON
January 10, 1955

NACA RM E54I29

NATIONAL ADVISORY COMMITTEE FOR AERONAUTICS

RESEARCH MEMORANDUM

EXPERIMENTAL INVESTIGATION OF A 0.4 HUB-TIP DIAMETER RATIO AXIAL-FLOW COMPRESSOR INLET STAGE AT TRANSONIC INLET RELATIVE MACH NUMBERS

II - STAGE AND BLADE-ELEMENT PERFORMANCE

By John C. Montgomery and Frederick W. Glaser

SUMMARY

An investigation was conducted to determine the feasibility of increasing the specific weight flow of a transonic axial-flow compressor inlet stage by decreasing the hub-tip ratio. A transonic axial-flow inlet stage with a hub-tip ratio of 0.4 was designed to produce a total-pressure ratio of 1.35 at a corrected specific weight flow of 34.9 pounds per second per square foot of rotor frontal area. The design and over-all performance of the rotor for the stage were reported previously in the first phase of this investigation. The current phase of the investigation was conducted to determine the blade-element and the over-all performance of the complete stage.

At design corrected tip speed of 1000 feet per second, the design stage total-pressure ratio of 1.35 was obtained at a corrected specific weight flow of 34.0 pounds per second per square foot of frontal area at an adiabatic efficiency of 0.86. Peak efficiencies of 0.88, 0.91, and 0.94 were obtained at 100, 80, and 60 percent design speed, respectively. Simplified design procedures which neglect entropy and curvature terms in the equations of motion are not sufficiently accurate for the determination of velocity distributions and flow angles in the design of transonic axial-flow compressor stages with low hub-tip ratios and high pressure ratios.

The increased loss at the rotor tip section for a low hub-tip ratio rotor may be attributed to increased loading for relative inlet Mach numbers up to 1.05. For the given rotor design, significant total-pressure losses attributable to mixing losses and probe errors existed.

The large losses experienced at the stator hub section were attributed to the radial inward shift of the outer-casing boundary layer and to the high inlet absolute Mach number.

INTRODUCTION

Turbojet engines with low ratios of engine weight to thrust must be developed for aircraft propulsion at high flight speeds. One method of increasing the engine thrust without appreciably increasing the engine weight is to increase the weight flow per unit frontal area through the engine. This can be accomplished by utilizing a transonic inlet stage in a multistage axial-flow compressor. Axial-flow compressor stages operating in the transonic region of relative inlet Mach number (refs. 1 and 2) produce high pressure ratio, high efficiency, and high weight flow per unit frontal area. In reference 2, a transonic inlet stage with a 0.5 hub-tip diameter ratio was designed to produce high pressure ratio, high efficiency, and high weight flow per unit frontal area. Further increases in weight flow per unit frontal area through a transonic inlet stage can be accomplished by either increasing the inlet axial Mach number or by decreasing the hub-tip diameter ratio. The transonic axial-flow compressor stage used in this investigation (ref. 3) was designed primarily to determine the feasibility of increasing the weight flow per unit frontal area by reducing the hub-tip diameter ratio to 0.4. The over-all performance of the rotor without the stator blades is presented in reference 3. The blade-element performance of the rotor, the blade-element performance of the stators, and the over-all performance of the stage based on detailed instrument surveys are presented herein. The rotor-blade-element data are presented for corrected tip speeds of 600, 800, 1000, and 1050 feet per second. The stator-blade-element data and the over-all stage performance data are presented for rotor corrected tip speeds of 600, 800, and 1000 feet per second.

APPARATUS AND PROCEDURE

Rotor Design

The rotor design is presented in detail in reference 3. Simple radial equilibrium conditions which neglect entropy and curvature terms in the equations of motion were assumed for velocity-distribution calculations. The rotor was designed to produce a pressure ratio of 1.35 at a specific weight flow of 34.9 pounds per second per square foot frontal area and a tip speed of 1000 feet per second. The diameter of the rotor was 14 inches, and the inlet hub-tip diameter ratio was 0.4. The design inlet relative Mach number varied from 0.70 at the hub to 1.10 at the tip. The rotor was designed for constant energy addition at all radii (vortex type) and employed double-circular-arc blade profile sections. At the time the rotor was designed, very limited data were available on the performance of the high-speed circular-arc blades. As a consequence, assumptions for the blade performance had to be made. One of these assumptions, which the blade-element performance data will show was not adequate, was that the optimum incidence angle at all radii was 3°. A summary of the rotor-blade design values and geometry is given in table I.

[redacted]

Stator Design

The stators for this inlet-stage investigation were designed to return the rotor-outlet air back to the axial direction so that high relative inlet Mach numbers could be obtained for succeeding stage designs. The stator design air inlet angle (measured from the axial direction) varied from 25.7° at the tip to 42.0° at the hub. The design inlet absolute Mach number varied from 0.638 at the tip to 0.784 at the hub. NACA 65-series blade profiles were used for the stators, and standard procedures as outlined in reference 4 were followed in selecting the blade section for each radius. A constant blade chord of 2 inches and a constant blade thickness-to-chord ratio of 0.06 were used. The stator-blade design values and geometry are presented in table II. In the table are included values of equivalent circular-arc camber and incidence angle which were obtained by approximating the NACA blade by a circular-arc blade of equal mean-line camber height and chord. The design stator-outlet annulus area was adjusted to maintain the design ratio of axial velocity to tip speed of 0.647 throughout the stage. The design outlet annulus was then arbitrarily increased 6 percent to allow for the assumed growth of the wall boundary layer.

3436

CV-1 back

Compressor Installation

The compressor installation is the same as that described in reference 3 except that stator blades were added to obtain the over-all stage and stator-blade-element performance.

Instrumentation

The axial measuring stations used to observe the stage performance conditions are shown in figure 1. Stations 1 (located 1/2 in. upstream of the rotor-blade hub leading edges) and 2 (located 1/2 in. downstream of the rotor-blade hub trailing edges) were used to observe the rotor-inlet and -outlet conditions, respectively. Station 3 (located 1 in. downstream of the stator-blade hub trailing edges) was used to observe the stator-outlet conditions.

Measurements at the three axial stations were made at five major radial stations located at 10, 30, 50, 70, and 90 percent of the blade passage height from the outer wall. Additional radial survey stations at each axial station were located from 2 to 7 percent of the blade passage height or within the boundary layer at both the hub and tip sections. Static-pressure taps were located on the outer and inner passage walls at each of the axial measuring stations.

[redacted]

At the rotor inlet (station 1), total pressure and air angle were measured at all radial survey stations including the stations in the boundary layer, whereas static pressure was measured at the five major radial stations and at the walls. At the rotor outlet (station 2), total temperature, total pressure, and angle were measured at all radial survey stations. Static pressure was measured at the five major radial stations and at the walls. In the investigation of the rotor alone, the total temperature after the rotor was measured at three circumferential positions, whereas in the complete stage investigation the total temperature after the rotor was measured at two circumferential positions.

Downstream of the stators (station 3) total temperature, total pressure, and angle were measured and recorded continually by an automatic recorder as each instrument was traversed circumferentially across one blade passage. Circumferential surveys were made at the five major radial positions; and at a few weight-flow points, measurements of total pressure and total temperature in the end regions were included. Static pressure was found to be constant circumferentially across the stator-blade-outlet passage and was therefore measured along a radial line at the five major stations. Static pressure was also observed at the walls.

Weight-flow and efficiency checks of the data indicated good reliability. The integrated weight flows measured at the three axial stations agreed within approximately 3 percent of the weight flow measured by the thin-plate orifice. The integrated mass-averaged adiabatic efficiencies agreed within approximately 3 percent of the integrated mass-averaged momentum efficiencies.

Procedure

The investigation was divided into two phases: (1) investigation of the rotor alone in which the rotor-blade-element performance was obtained and (2) the complete-stage investigation in which the stator-blade-element and over-all stage performances were obtained. The data for the rotor alone were taken at corrected speeds of 60, 80, 100, and 105 percent of design speed; whereas the complete-stage and stator data were taken at corrected speeds of 60, 80, and 100 percent of design speed. Rotor and stage over-all performances were obtained by mass averaging the radial performances at a given axial station. For the given rotor and stage, the arithmetically averaged over-all performances were found to be equivalent to the more rigorous mass-averaged over-all performances and are presented to be consistent with the data presented in reference 3.

Computations and Symbols

The symbols and equations used in computing the blade-element and stage performances are included in appendixes A and B, respectively. An illustration of the air and blade angles used in the symbols and equations is shown in figure 2.

OVER-ALL PERFORMANCE

Over-all Performance of Rotor and Stage

The over-all performance of the rotor with and without stator blades is presented in figure 3 for corrected tip speeds of 600, 800, and 1000 feet per second. For the blade-element investigation of the rotor alone, an overspeed run of 5 percent was made.

At the design corrected tip speed of 1000 feet per second, for the rotor alone, the rotor design total-pressure ratio of 1.35 was obtained at a corrected specific weight flow of 34.4 pounds per second per square foot of frontal area and at an adiabatic efficiency of 0.87. Allowing for the inlet boundary-layer blockage factor of 0.98 (ref. 3), which was not considered in the rotor design, the specific weight flow compared favorably with the design specific weight flow of 34.9 pounds per second per square foot of frontal area. Although a rotor peak adiabatic efficiency of 0.93 was obtained at design speed, an efficiency of only 0.87 was obtained at design speed and pressure ratio. Peak rotor efficiencies of 0.98 and 0.96 were obtained for the 80 and 60 percent design speeds, respectively. At 5 percent overdesign speed, the rotor had a peak efficiency of 0.91 at a total-pressure ratio of 1.44.

For the complete-stage investigation, the pressure ratio of 1.35 was obtained at a specific weight flow of 34.0 pounds per second per square foot of frontal area and at an adiabatic efficiency of 0.86. Peak stage efficiency at design speed was approximately 0.88 and occurred at a specific weight flow of 33.3 pounds per second per square foot of frontal area. Peak stage efficiencies of 0.91 and 0.94 were obtained for the 80 and 60 percent design speeds, respectively.

The stators, in general, only slightly decreased the efficient operating range of the rotor. The stage peak efficiency was approximately 1, 7, and 5 percent less than the rotor peak efficiencies for 60, 80, and 100 percent design speeds, respectively.

Stage and rotor performances at each tip speed were limited to weight flows above those at which blade vibrations were indicated. Although the magnitude of the vibrations encountered was small, performances at the lower weight flows were not investigated because of possible blade failure.

The over-all total-pressure ratio determined for the investigation of the rotor alone in reference 3 was found to be less than the over-all total-pressure ratio determined from the present blade-element performance investigation (fig. 4). The only variation between the two investigations is that in reference 3 the rotor-outlet conditions were measured at station 3, whereas in the present blade-element investigation the rotor-outlet conditions were measured at station 2. This loss in total pressure may be attributed to (1) losses associated with boundary-layer growth on the outer casing, (2) mixing losses associated with the nonuniform flow leaving the rotor, and (3) probe errors due to the nonsteady flow.

Evaluation of Total-Pressure Loss

Calculations indicated that the boundary-layer growth on the outer casing would not cause the magnitude of pressure losses obtained. The magnitude of the mixing losses associated with the nonuniform flow leaving the rotor is unknown. However, the mixing losses can be qualitatively evaluated by the method of reference 5, in which the two-dimensional mixing losses associated with the flow leaving a blade row are analyzed. Reference 5 points out that for the two-dimensional compressible case (in the region of Mach number encountered) mixing losses represent an increase of approximately 20 to 40 percent over the blade pressure losses measured immediately downstream of a blade row. In the blade end region where the two-dimensional analysis of reference 5 breaks down, the mixing losses are probably greater.

The magnitude of the probe errors involved in measuring the total pressure downstream of a rotating blade row is also unknown. However, calculations show (under certain assumptions) that the magnitude of the probe errors may be in the same order of magnitude as the mixing losses. The magnitude of both the mixing loss and probe error is a function of the wake profile leaving the blade row.

For a given speed the measured total-pressure loss between stations 2 and 3 increased with radius as shown for design speed in figure 5. Since the rotor efficiency decreases toward the rotor tip section, it is possible that the flow at the tip section is nonuniform and therefore caused greater mixing losses and probe errors. It will be shown in the blade-element performance analysis that the rotor tip-section peak efficiency was indicated as 0.81. This tip-section efficiency is approximately 10 points lower than the rotor tip-section peak efficiency of other transonic rotors (e.g., ref. 6) and therefore may cause pressure losses which under better flow conditions would not exist.

A total-pressure-loss coefficient (eq. (9)) similar to the total-pressure-loss coefficient used for stator blades was determined for the

measured loss between stations 2 and 3. The loss coefficient was taken as the ratio of the total-pressure loss to the difference of the total and static pressures at the rotor outlet. The total-pressure-loss coefficient thus described was obtained from the data of figure 5 and is shown in figure 6. In the tip region the measured total-pressure-loss coefficient reaches a value of 0.18. The magnitude of the total-pressure-loss coefficient for the given rotor is high, and it points out the necessity of a more accurate knowledge of associated mixing losses and probe errors behind the rotor-blade row.

BLADE-ELEMENT PERFORMANCE

Rotor-Blade-Element Performance

The over-all performance of the rotor indicated that rotor design weight flow and pressure ratio were obtained, but that design efficiency was not. In order to further analyze the performance of the rotor, an investigation of the rotor-blade-element performance is required.

The rotor-blade-element performance characteristics are presented for corrected tip speeds of 600, 800, 1000, and 1050 feet per second in figures 7 to 13. The data were determined from the investigation of the rotor alone from measurements at axial stations 1 and 2.

Inlet Conditions

In the design of the rotor, conditions of isentropic flow with no curvature in the flow passage were assumed at the rotor inlet and, therefore, radial constant axial velocity was predicted. The actual axial velocity at the rotor inlet was not constant radially and is presented in figure 7 as a plot of the ratio of axial velocity to mean-radius axial velocity for the specific weight flows near peak efficiency at each tip speed. The variation between the actual and the design constant axial-velocity distribution can be attributed to the effect of streamline curvature.

The variation of the relative inlet air angle against radius is presented in figure 8. The curves are presented for various weight-flow points at each tip speed. The design relative inlet air angles and the design inlet blade angles are included on the curves for the design speed. The difference between the experimental relative inlet air angles and the design relative inlet air angle is a result of the off-design axial-velocity distribution. At design speed the incidence angle (relative inlet air angle minus the blade inlet angle) varied from 1° to 5° higher than the design value of 3° at all radii.

Rotor-Blade-Element Characteristics

The rotor-blade-element performance characteristics (deviation angle, total-pressure-loss coefficient, relative inlet Mach number, diffusion factor, axial-velocity ratio, efficiency, and work coefficient) are presented in figure 9 as a function of incidence angle. The data are presented for the five major radial stations from hub to tip. Extensive data are presented to describe in detail the performance of the rotor and to further supplement the limited published data on transonic-rotor-blade performance.

There is no apparent trend to the variation of the deviation angle with tip speed within the range investigated. At minimum-loss incidence angle at all radii, the deviation angles for all tip speeds agreed within approximately $1\frac{1}{2}^{\circ}$ of the values predicted by Carter's Rule $\left(\Delta = m\varphi\sqrt{\frac{1}{\sigma}}\right)$ (ref. 7). At the lower incidence angles, the deviation angles tend to increase, and this increase coincided with the sharp increase of the axial-velocity ratio across the blade section.

The low-loss region of the relative total-pressure-loss coefficient (eq. (3)) contracts and shifts to higher values of incidence angle as the speed (relative inlet Mach number) is increased. At design speed (fig. 9), the incidence angle corresponding to minimum loss increased from approximately 4° at the rotor tip to 8° at the rotor hub section. As shown in figure 8, the rotor incidence angle at design speed and at near peak-efficiency weight flow also varied from approximately 4° at the rotor tip section to 8° at the hub section. Thus it appears that the rotor blade was actually operating near the minimum-loss incidence angle at all radii, although the assumed design incidence angle at all radii was 3°. As shown by figure 9, the minimum-total-pressure-loss coefficient at design speed was approximately 0.025 for all radii except for the tip section, where it increased to approximately 0.14. Excluding the tip section, the value of the minimum-total-pressure-loss coefficient obtained is of the same magnitude experienced in other transonic rotor designs (ref. 8).

The marked increase of the total-pressure-loss coefficient at the tip section can be attributed to either increased blade loading or shock losses resulting from the high inlet relative Mach number. The effect of Mach number and blade loading can be qualitatively evaluated by means of the diffusion factor of reference 9. For rotor tip sections (approximately 10 percent of the blade height from the outer wall) reference 9 presents a range or band of total-pressure-loss coefficient against diffusion factor data for rotors operating below the inlet relative Mach number at which large shock losses occur. At design speed the rotor-tip-section total-pressure-loss coefficients corresponding to the low-loss incidence-angle range of figure 9 were compared with the data of

reference 9. By neglecting the low-incidence-angle point (maximum-weight-flow point), three of the four points fall within the prescribed range; the fourth point fell just outside the band. The corresponding maximum relative inlet Mach number was approximately 1.05. In reference 8 the total-pressure-loss coefficients for the rotor tip section fell within the prescribed band of reference 9 for relative inlet Mach numbers up to 1.15. It is therefore believed that the increased losses at the rotor tip section can still be attributed to the increase in blade loading or diffusion factor and the associated end losses and not to the increased level of the relative inlet Mach number. The increased diffusion factor at the tip-section low-loss incidence-angle range can be attributed to the decrease in the axial velocity across the blade at that section. From the equation for the diffusion factor (eq. (6)), the magnitude of the diffusion factor for a given value of turning (ΔV_θ) increases as the ratio of the axial velocity across the blade and therefore V_2'/V_1' are decreased.

The variation of inlet relative Mach number with incidence angle is included in figure 9. At design speed the relative inlet Mach number corresponding to the minimum-loss incidence angle varied from approximately 0.65 at the hub to 1.05 at the tip.

The diffusion factor, in general, increased slightly with speed in the low-loss region of incidence angle. Since the diffusion factor (ref. 9) and the associated values of the total-pressure-loss coefficient only pertain to the low-loss incidence-angle range, the magnitudes of the diffusion factor outside this range are relatively unimportant.

The variation of rotor work input with incidence angle is presented in figure 9 as a dimensionless work coefficient (eq. (5)). At incidence angles corresponding to the minimum-loss region, the work-input coefficient varied little with speed.

The blade-element efficiency at optimum incidence angle varied primarily with the magnitude of the total-pressure-loss coefficient. Blade-element efficiency at optimum incidence angle (eq. (6)), which is a function of work input, inlet relative Mach number, and total-pressure-loss coefficient, approached 100 percent over the greater portion of the blade but decreased to 80 percent at the tip section for the higher speeds.

Rotor-Blade-Outlet Conditions

Absolute Mach number, absolute air angle, and axial-velocity distribution at the rotor outlet are presented in figures 10 to 12 as a function of radius. In figures 10 and 11 the data are presented for several weight-flow points for each tip speed. In figure 12 the data are presented for two weight-flow points at design speed only. On the curves

of absolute outlet air angle for design speed (fig. 10), the design stator-inlet air angles and the design stator-blade-inlet air angles are included. At the specific weight flow corresponding to peak efficiency (approximately 33.72 lb/(sec)(sq ft) of frontal area), the absolute rotor-outlet air angle (and therefore the stator-inlet air angle) varied from 1° to 10° higher than the design values shown in figure 10 or in table II. This variation can be attributed to the nonuniform axial-velocity distribution at the rotor outlet. Absolute rotor-outlet Mach number (fig. 11) at design speed and near-peak-efficiency weight flow increased from approximately 0.61 at the tip section to 0.80 at the hub section. The variation of absolute Mach number with radius at other tip speeds and weight flows was similar, but the level of the Mach number gradient varied.

The radial distribution of the outlet axial velocity at design speed and near-peak-efficiency weight flows is presented in figure 12 as a ratio of the axial velocity to the mean-radius axial velocity. The difference between the actual and the design constant axial-velocity distributions can be attributed to the effect of streamline curvature and entropy gradients which were assumed negligible in the simplified design procedure (simple radial equilibrium conditions). In order to evaluate the effects of streamline curvature on the axial-velocity distribution, the procedure outlined in reference 10 was followed. Included in figure 12 is the axial-velocity distribution predicted by the simple radial equilibrium equation with entropy gradients (ref. 10) as applied to the measured rotor-outlet conditions. The difference between the radial equilibrium solution with entropy gradients and the actual velocity distribution can be attributed to the effect of streamline curvature which is neglected in the solution.

In order to verify the effect of hub curvature on the axial-velocity distribution at the rotor outlet, the axial-velocity distribution was determined experimentally by replacing the rotor with a dummy hub section (blades removed) and drawing air through the unit. The axial-velocity distribution thus obtained is presented in figure 13. The difference between the experimental radial velocity distribution obtained with the dummy rotor hub section and the constant axial velocity, figure 13, can be attributed to the effect of hub curvature at the rotor outlet. In comparing figures 12 and 13 it can be seen that the magnitude of the effect of curvature on radial axial-velocity distribution as determined by simple radial equilibrium with entropy gradients (with rotor) and experimental results with the rotor removed are comparable. The Mach number at the rotor outlet in both cases was equivalent. For the given rotor, hub curvature caused approximately 8 percent maximum variation in radial axial-velocity distribution. In the design of low hub-tip ratio rotors with high pressure ratio, radial axial-velocity distributions of this magnitude should be taken into account.

The blockage factor for the rotor outlet at design speed varied little with weight flow and at rotor over-all peak efficiency was approximately 0.97.

STATOR-BLADE-ELEMENT PERFORMANCE

The stator-blade-element performance characteristics are presented for corrected tip speeds of 600, 800, and 1000 feet per second. The data were obtained from the investigation of the complete stage from measurements 1/2 inch upstream and 1 inch downstream of the stator blades.

Inlet Conditions

The stator-inlet conditions or the rotor-outlet conditions for the investigation of the complete stage varied little from the rotor-outlet conditions obtained from the investigation of the rotor alone for a given speed and flow. The rotor-outlet conditions (figs. 10 to 12) can therefore be taken as the stator-blade-inlet conditions.

Blade-Element Characteristics

The blade-element characteristics of the stator blades are presented in figure 14. The data are presented at three tip speeds for the five major radial stations from hub to tip.

The stator total-pressure-loss coefficient (eq. (7)) is defined as the ratio of the difference between the outlet free-stream total pressure and the averaged total pressure to the difference between the inlet total and static pressures. As in the case of reference 8, the free-stream total pressure was taken as the average of the free-stream pressure outside of the wake region. In the case of the hub region where a clear distinction of wake regions could not be made, the free-stream pressure was taken as the maximum free-stream pressure. Hub-section losses may therefore appear somewhat large. A typical variation of the measured total pressure at the stator outlet from hub to tip is presented in figure 15. The total-pressure distributions presented in the figure are for the near-peak-efficiency weight flow at design speed. As demonstrated by the hub-section total-pressure distribution, no clear distinction can be made between the wake region and the free-stream pressure.

For all sections except the hub region, increasing the Mach number to approximately 0.7 had little effect on the magnitude of the minimum value of the stator loss coefficient. The increase of Mach number did, however, tend to reduce the low-loss incidence-angle range.

[redacted]

The optimum incidence angle for all blade sections excluding the hub section corresponded to the design incidence angles (table II) used in the stator design. However, the stator tip section (fig. 10) operated at off-design inlet air angles (and therefore off-design incidence angles) in the range of specific weight flows corresponding to over-all peak stage efficiency. Since the total-pressure-loss coefficient remained relatively constant over a large range of incidence angles at the stator tip section (fig. 15), the stator tip sections still operated in a region of relatively low loss at the off-design incidence angles.

The magnitude of the minimum total-pressure-loss coefficient increased sharply at the stator hub section. At the equivalent tip speed of 600 feet per second, the minimum loss at the hub section was approximately twice the minimum loss at design speed for the other blade sections. The magnitude of the total-pressure-loss coefficient at the hub section also increased sharply with tip speed and at design speed reached a value of 0.175. From figure 14, the stator diffusion factor (eq. (8)) at optimum incidence angle increased from a maximum value of approximately 0.35 at the tip section to 0.6 at the hub section. Reference 9, however, shows that for stator blades an increase of the diffusion or blade-loading factor up to 0.6 does not cause increased values of the total-pressure-loss coefficient. It appears, therefore, that the increased loss at the stator hub section is not an effect of diffusion factor. The increased loss at the stator-blade hub section must therefore be attributable to (1) separation of the boundary layer at the hub, (2) Mach number, and (3) the radial inward shift of the outer-casing boundary layer caused by the static-pressure distribution within the blade passages.

Separation of the boundary layer seems feasible because of the sharp change in the slope of the hub (fig. 1) at the stator inlet. However, a subsequent investigation of the stator-blade performance with a redesigned hub section (gradual change in hub curvature) did not appreciably reduce the loss at the stator-blade hub section.

The stator-blade critical inlet Mach number was calculated for the hub section at design conditions. For the given blade configuration the minimum throat area occurred upstream of the blade passage, and the corresponding critical inlet Mach number at which a Mach number of 1.0 was reached at the minimum throat area was calculated to be approximately 0.75. The actual inlet Mach number for the stator hub section at design conditions (design incidence angle) was 0.82 at 100 percent design speed and 0.715 at 80 percent design speed (fig. 14). Since large losses were experienced at both 80 and 100 percent design speeds and since the critical inlet Mach number was based on the minimum throat area upstream of the blade passage, it is not definite whether or not a choking condition existed.

[redacted]

It is also possible that the increased losses at the stator hub section were caused by the radial inward shift of the casing boundary-layer air. As the casing boundary layer enters the tip section of the stator-blade passages, it is unable to support the static-pressure gradient dp/dn imposed upon it by the curved path (tangential direction) of the free-stream velocity within the stator passages. Consequently, since $\frac{dp}{dn} = \rho \frac{V^2}{r_c}$, the radius of curvature must decrease when the velocity at the outer wall decreases. The decrease in the radius of curvature causes the casing boundary-layer air to collect on the suction surface of the stator-blade tip sections. When the boundary layer on the blade suction surface at all other radii is sufficiently large, the radial static-pressure distribution (imposed by the upstream absolute whirl velocity) forces the air radially inward toward the stator-blade hub section.

The stator deviation angle varied little with incidence angle or tip speed in the region of low-loss total-pressure coefficient. At optimum incidence angle the deviation angle at all blade sections except the hub were within 1° of the design value (table II).

The sharp decrease in the axial-velocity ratio across the stator blades at the hub section can be attributed to decrease in flow through that region of the blades. The decrease in flow is caused by the increased total-pressure losses.

Outlet Condition

The variation of the stator-outlet absolute Mach number, the absolute turning angle, and the total-pressure-loss coefficient are plotted against radius in figures 16 to 18. The data are presented for three corrected specific weight flows at each tip speed. As shown by figure 16, approximately axial air flow as indicated by the outlet air angles of zero were obtained at all radii for all tip speeds and specific weight flows.

The total-pressure-loss coefficient (fig. 18) increased sharply at the blade hub section for all tip speeds. As previously pointed out, the increased loss at the hub section may be attributed to the radial inward shift of the outer-casing boundary layer or to Mach number. The increased loss at the stator tip section principally at design speed was caused by operation of the blade section at off-design incidence angles. The increased loss at the tip section within 0.25 inch from the wall for the lower speeds can be attributed to boundary-layer losses.

The outlet blockage factor at design speed for the stators varied slightly with weight flow and was approximately 0.94 for over-all stage peak-efficiency weight flow.

SUMMARY OF RESULTS

The following results were obtained from the blade-element investigation of the performance of a 0.4 hub-tip ratio transonic axial-flow stage.

1. At design corrected tip speed of 1000 feet per second, the design stage total-pressure ratio of 1.35 was obtained at a corrected specific weight flow of 34.0 pounds per second per square foot of frontal area and an adiabatic efficiency of 0.86. Peak efficiencies of 0.88, 0.91, and 0.94 were obtained at 100, 80, and 60 percent design speeds, respectively.

2. Simplified design procedures for the rotor which neglect entropy gradients and curvature terms in the equations of motion were not sufficiently accurate for the determination of velocity distribution and flow angles in the design of transonic axial-flow stages with low hub-tip ratios and high pressure ratios.

3. The increased loss at the tip section for low hub-tip ratio rotors may still be attributed to increased blade loading or diffusion factor for relative inlet Mach numbers up to 1.05.

4. At design-speed over-all peak efficiency, the rotor-blade sections operated at optimum but off-design incidence angles.

5. For the given rotor design in which the rotor tip-section peak efficiency was 0.81, significant measured total-pressure loss attributable to mixing losses and probe errors were found to exist.

6. The rotor-blade-element deviation angles at minimum loss were within $1\frac{1}{2}^{\circ}$ of the values predicted by Carter's Rule.

7. The large losses experienced at the stator hub were attributed to the radial inward shift of outer-casing boundary layer and to Mach number. The increased losses experienced at the stator tip section were caused by mismatching of stator incidence angles at that section.

Lewis Flight Propulsion Laboratory
National Advisory Committee for Aeronautics
Cleveland, Ohio, September 29, 1954

[redacted]

APPENDIX A

SYMBOLS

The following symbols are used in this report:

A,B,C,D,E	blade radial measuring stations
A_f	compressor frontal area, sq ft
C_L	coefficient of lift
c_p	specific heat of air at constant pressure, Btu/(lb)(^oR)
D	diffusion factor
g	acceleration due to gravity, 32.17 ft/sec^2
H	total enthalpy, ft-$\overline{lb}$/lb
i	angle of incidence, angle between tangent to blade mean camber line at leading edge and inlet air direction, deg
J	mechanical equivalent of heat, 778 ft-lb/Btu
M	Mach number
m	variable in Carter's rule
n	direction normal to streamline
P	total pressure, lb/sq ft
p	static pressure, lb/sq ft
r	radius, in.
r_c	radius of curvature of streamline, in.
T	total temperature, ^oR
t	static temperature, ^oR
U	blade speed, ft/sec
V	velocity of air, ft/sec
W	weight flow, lb/sec

[redacted]

z radius ratio, r/r_t

α angle of attack, angle between blade chord and inlet air, deg

β angle between velocity vector and rotor axis, deg

γ ratio of specific heats

δ ratio of inlet pressure to standard NACA sea-level pressure, $P/2116.2$

δ^o deviation angle, angle between tangent to mean camber line at blade trailing edge and air direction, deg

η adiabatic efficiency

θ ratio of inlet total temperature to standard NACA sea-level temperature, $T/518.6$

ρ static air density, slugs/cu ft

σ solidity ratio, ratio of blade chord to blade spacing

φ blade camber angle, deg

π blade inlet angle, angle between tangent to blade mean line and rotor axis at blade leading edge, deg

ω total-pressure-loss parameter

Subscripts:

av average

b blade element

f free stream

M mixing loss and probe error

m mean

R rotor

S stator

t tip

[redacted]

z axial direction

θ tangential direction

0 compressor depression tank

1 rotor inlet

2 rotor outlet (stator inlet)

3 stator outlet

Superscript:

' relative to rotor

APPENDIX B

EQUATIONS

The equations used for the blade-element and over-all performance are included below.

Complete stage. - The over-all arithmetical-averaged adiabatic efficiency for the complete stage is

$$\eta = T_1 \sum_{n=1}^{n} \frac{1}{n} \left[\frac{\left(\frac{P_3}{P_1}\right)^{\frac{\gamma-1}{\gamma}} - 1}{T_3 - T_1} \right] \tag{1}$$

The over-all arithmetical-averaged total-pressure ratio is

$$\frac{P_3}{P_1} = \sum_{n=1}^{n} \frac{1}{n} \frac{P_3}{P_1} \tag{2}$$

Rotor-blade element. - The equation for the rotor-blade-element relative total-pressure coefficient (ref. 9) is

$$\omega_R = \left(\frac{P_2'}{P_1'}\right)_{ideal} \left\{ \frac{1 - \left(\frac{P_2}{P_1}\right)\left(\frac{T_1}{T_2}\right)^{\frac{\gamma}{\gamma-1}}}{1 - \left[1 + \frac{\gamma - 1}{2} (M_1')^2\right]^{-\frac{\gamma}{\gamma-1}}} \right\} \tag{3}$$

where $\left(\frac{P_2'}{P_1'}\right)_{ideal} = \left\{ 1 + \frac{\gamma - 1}{2} M_r'^2 \left[1 - \left(\frac{r_1}{r_2}\right)^2 \right] \right\}^{\frac{\gamma}{\gamma-1}} \approx 1$ for given rotor

3436

design and M_r is the wheel rotational Mach number (outlet wheel tangential velocity divided by inlet relative stagnation velocity of sound).

The blade-element adiabatic efficiency is

$$\eta_b = \frac{T_1\left[\left(\frac{P_2}{P_1}\right)^{\frac{\gamma-1}{\gamma}} - 1\right]}{T_2 - T_1} \tag{4}$$

In terms of ω, M_1', and T_2/T_1, the blade-element adiabatic efficiency (ref. 6) is for $\left(\frac{P_2'}{P_1'}\right)_{ideal} = 1.0$

$$\eta_b = \frac{\frac{T_2}{T_1}\left(1.0 - \omega_R\left\{1.0 - \left[1.0 + \frac{\gamma-1}{2}(M_1')^2\right]^{-\frac{\gamma}{\gamma-1}}\right\}\right)^{\frac{\gamma-1}{\gamma}} - 1.0}{\left(\frac{T_2}{T_1} - 1.0\right)}$$

The following is the equation for the dimensionless work coefficient (ref. 6):

$$\frac{\Delta H}{U_t^2} = \frac{Jgc_pT_{standard}\left(\frac{T_3}{T_1} - 1\right)}{\left(\frac{U_t}{\sqrt{\theta}}\right)^2} \tag{5}$$

The diffusion factor (ref. 9) is

$$D_R = \left(1 - \frac{V_2'}{V_1'}\right) + \frac{V_{\theta,1}' - V_{\theta,2}'}{2V_1'\sigma_R} \tag{6}$$

Stator-blade element. - The total-pressure-loss coefficient for the stator-blade element is

$$\omega_S = (P_{3,f} - P_{3,av})/(P_2 - p_2) \tag{7}$$

[redacted]

The equation for the diffusion factor (ref. 9) is

$$D_S = \left(1 - \frac{V_3}{V_2}\right) + \frac{V_{\theta,2} - V_{\theta,3}}{2V_2\sigma_S} \tag{8}$$

Rotor-alone performance. - The mixing-loss and probe-error total-pressure-loss coefficient for the investigation of the rotor alone is

$$\omega_{R,M} = \frac{P_2 - P_3}{P_2 - p_2} = \frac{\frac{P_2}{P_1} - \frac{P_3}{P_1}}{\frac{P_2}{P_1}\left(1 - \frac{p_2}{P_2}\right)} \tag{9}$$

3436

REFERENCES

1. Robbins, William H., and Glaser, Frederick W.: Investigation of an Axial-Flow Compressor Rotor with Circular-Arc Blades Operating up to a Rotor-Inlet Relative Mach Number of 1.22. NACA RM E53D24, 1953.

2. Lieblein, Seymour, Lewis, George W., Jr., and Sandercock, Donald M.: Experimental Investigation of an Axial-Flow Compressor Inlet Stage Operating at Transonic Relative Inlet Mach Numbers. I - Over-All Performance of Stage with Transonic Rotor and Subsonic Stators up to Rotor Relative Inlet Mach Number of 1.1. NACA RM E52A24, 1952.

3. Serovy, George K., Robbins, William H., and Glaser, Frederick W.: Experimental Investigation of a 0.4 Hub-Tip Diameter Ratio Axial-Flow Compressor Inlet Stage at Transonic Inlet Relative Mach Numbers. I - Rotor Design and Over-All Performance at Tip Speeds from 60 to 100 Percent of Design. NACA RM E53I11, 1953.

4. Herrig, L. Joseph, Emery, James C., and Erwin, John R.: Systematic Two-Dimensional Cascade Tests of NACA 65-Series Compressor Blades at Low Speeds. NACA RM L51G31, 1951.

5. Stewart, Warner L.: Investigation of Compressible Flow Mixing Losses Obtained Downstream of a Blade Row. NACA RM E54I20 , 1955.

6. Schwenk, Francis C., Lieblein, Seymour, and Lewis, George W., Jr.: Experimental Investigation of an Axial-Flow Compressor Inlet Stage Operating at Transonic Relative Inlet Mach Numbers. III - Blade-Row Performance of Stage with Transonic Rotor and Subsonic Stator at Corrected Tip Speeds of 800 and 1000 Feet Per Second. NACA RM E53G17, 1953.

[redacted]

7. Carter, A. D. S., and Hughes, Hazel P.: A Theoretical Investigation into the Effect of Profile Shape on the Performance of Aerofoils in Cascades. Power Jet Rep. R.1192, Res. and Dev., Power Jets, Ltd., Mar. 1946.

8. Sandercock, Donald M., Lieblein, Seymour, and Schwenk, Francis C.: Experimental Investigation of an Axial-Flow Compressor Inlet Stage Operating at Transonic Relative Inlet Mach Numbers. IV - Stage and Blade-Row Performance of Stage with Axial-Discharge Stators. NACA RM E54C26, 1954.

9. Lieblein, Seymour, Schwenk, Francis C., and Broderick, Robert L.: Diffusion Factor for Estimating Losses and Limiting Blade Loadings in Axial-Flow-Compressor Blade Elements. NACA RM E53D01, 1953.

10. Hatch, James E., Giamati, Charles C., and Jackson, Robert J.: Application of Radial-Equilibrium Condition to Axial-Flow Turbomachine Design Including Consideration of Change of Entropy with Radius Downstream of Blade Row. NACA RM E54A20, 1954.

[redacted]

TABLE I. - ROTOR-BLADE DESIGN VALUES AND GEOMETRY

Passage height, percent	Rotor-inlet radius ratio, z_1	Rotor-outlet radius ratio, z_2	Rotor-inlet relative air angle, β_1', deg	Rotor-outlet relative air angle, β_2', deg	Deviation angle, δ^o, deg	Blade camber angle, φ, deg	Blade maximum thickness ratio, t/C	Solidity ratio, σ	Angle of incidence, i, deg
100(tip)	1.000	1.000	57.1	46.8	2.1	9.4	0.0500	0.910	3.0
75	.85	.884	52.7	39.4	4.4	14.7	.0575	1.050	3.0
50	.70	.767	47.3	28.9	7.1	22.5	.0650	1.243	3.0
25	.55	.651	40.4	15.1	8.4	30.7	.0725	1.527	3.0
0(hub)	.40	.534	31.7	-4.2	9.2	42.1	.0800	1.990	3.0

TABLE II. - STATOR-BLADE DESIGN VALUES AND GEOMETRY

Passage height, percent	Stator-inlet radius ratio, z_2	Stator-outlet radius ratio, z_3	Stator-inlet air angle, β_2	Stator-outlet air angle, β_3	Lift coefficient, C_L	Angle of attack, α, deg	Deviation angle, δ^o, deg	Blade camber angle, φ, deg	Blade maximum thickness ratio, t/C	Solidity ratio, σ	Angle of incidence, i, deg
100(tip)	1.000	1.000	25.7	0	1.54	14.6	8.2	38.6	0.060	0.955	-4.7
75	.884	.893	28.5	0	1.80	16.0	7.5	40.0	.060	1.076	-4.0
50	.767	.785	32.0	0	1.70	18.0	7.2	42.4	.060	1.231	-3.2
25	.651	.678	36.4	0	1.82	20.6	6.9	45.4	.060	1.440	-2.1
0(hub)	.534	.570	42.0	0	1.97	24.3	6.8	49.0	.060	1.733	-.2

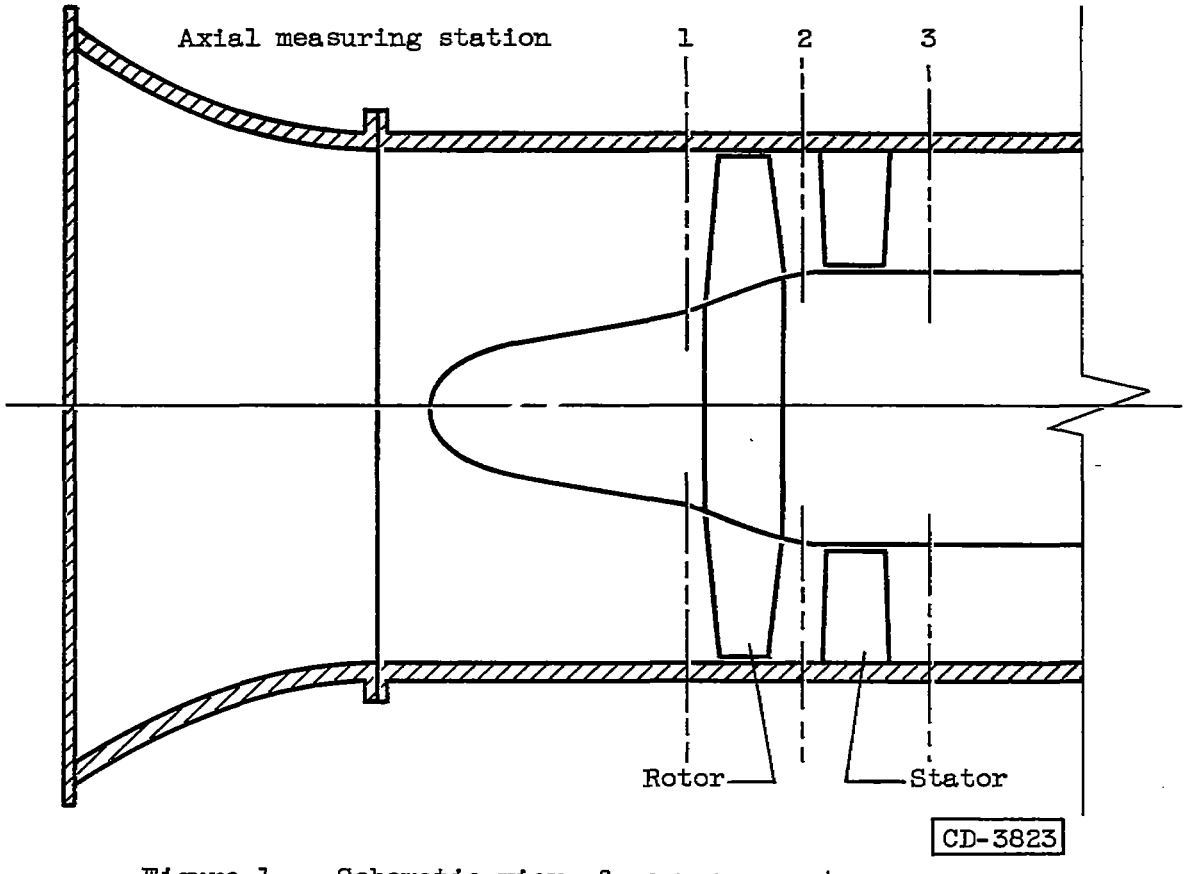

Figure 1. - Schematic view of compressor stage passage.

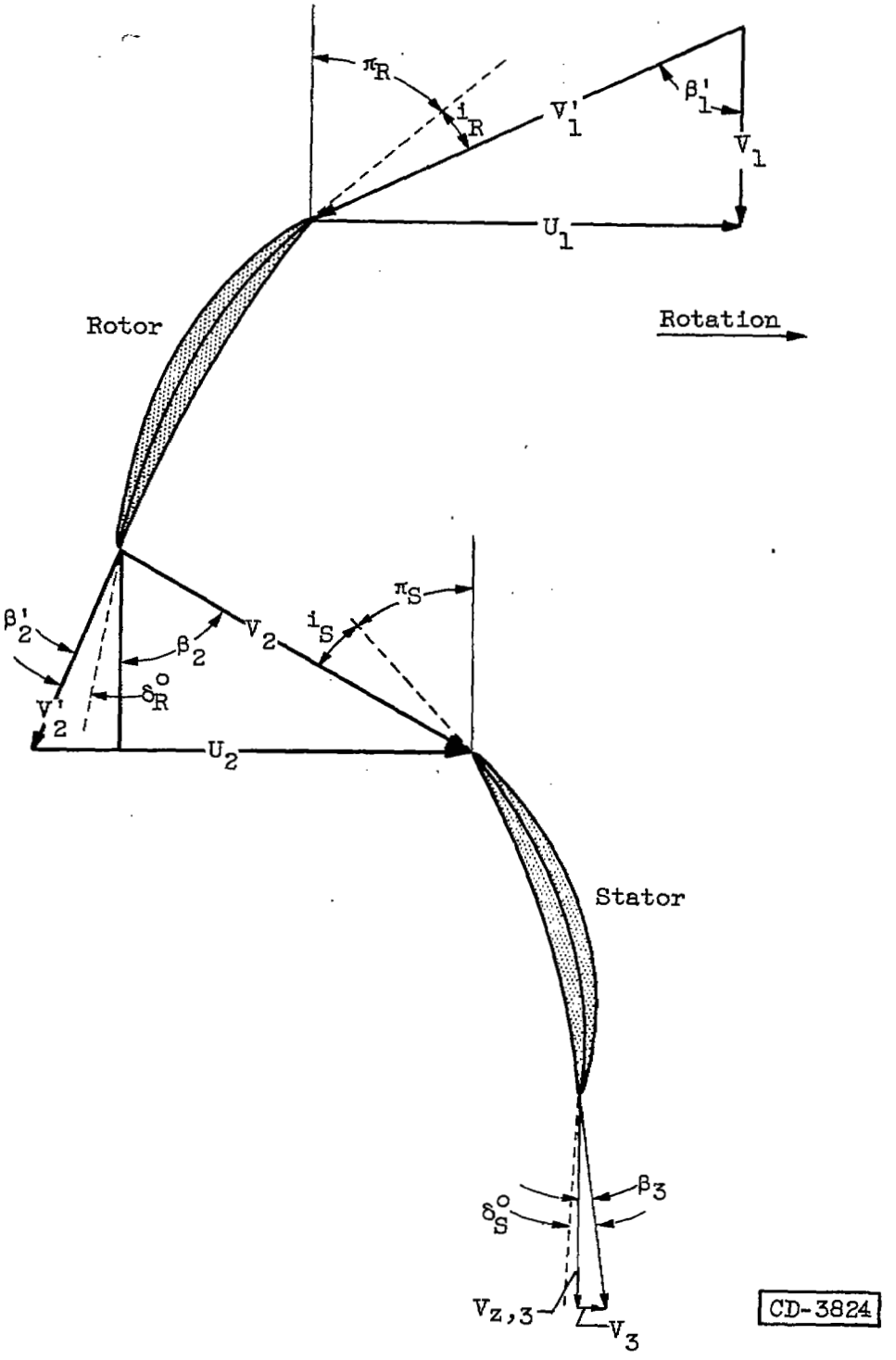

Figure 2. - Air and blade angles for a blade element.

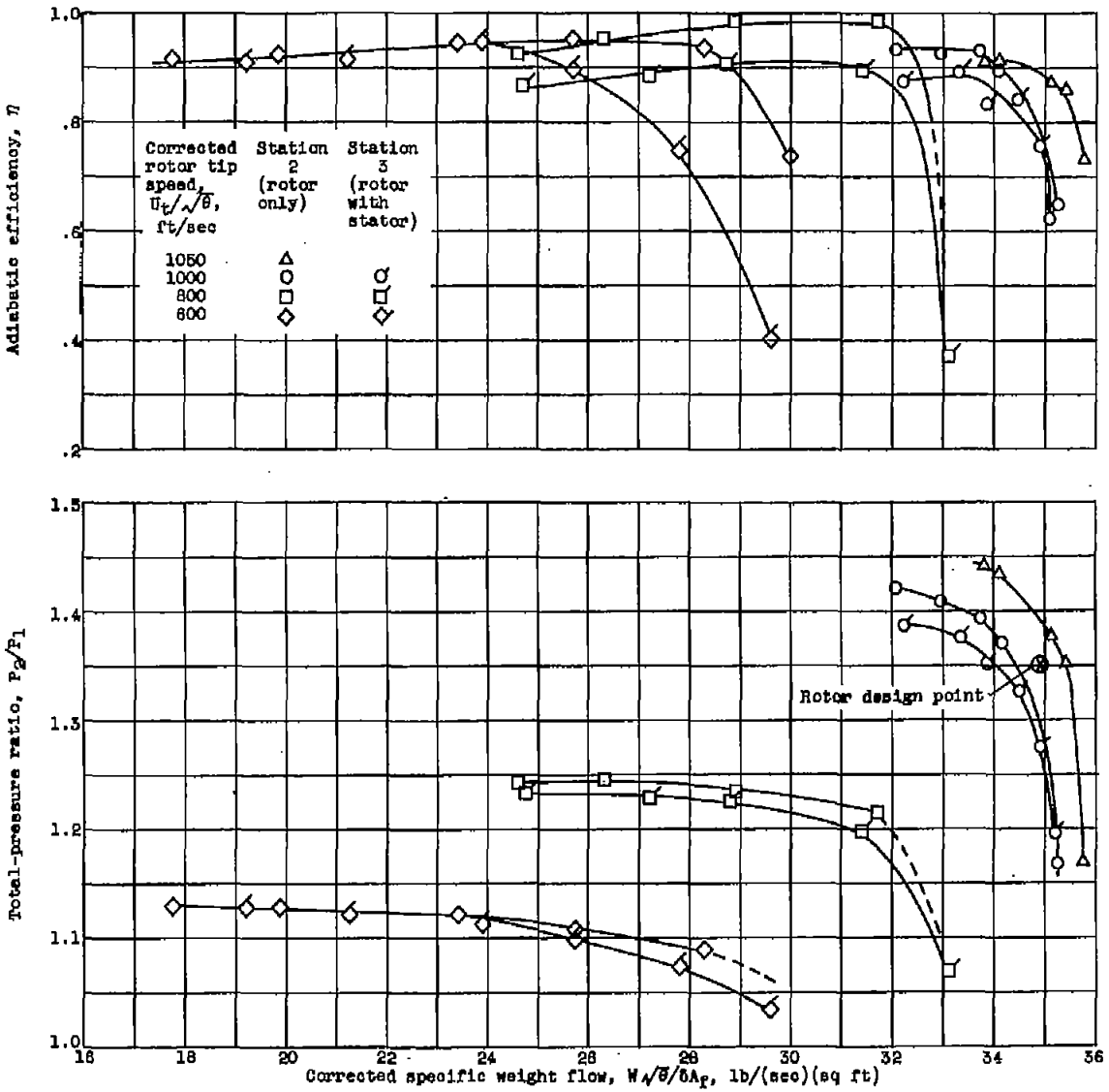

Figure 3. - Arithmetic-averaged over-all performance of rotor with and without stators.

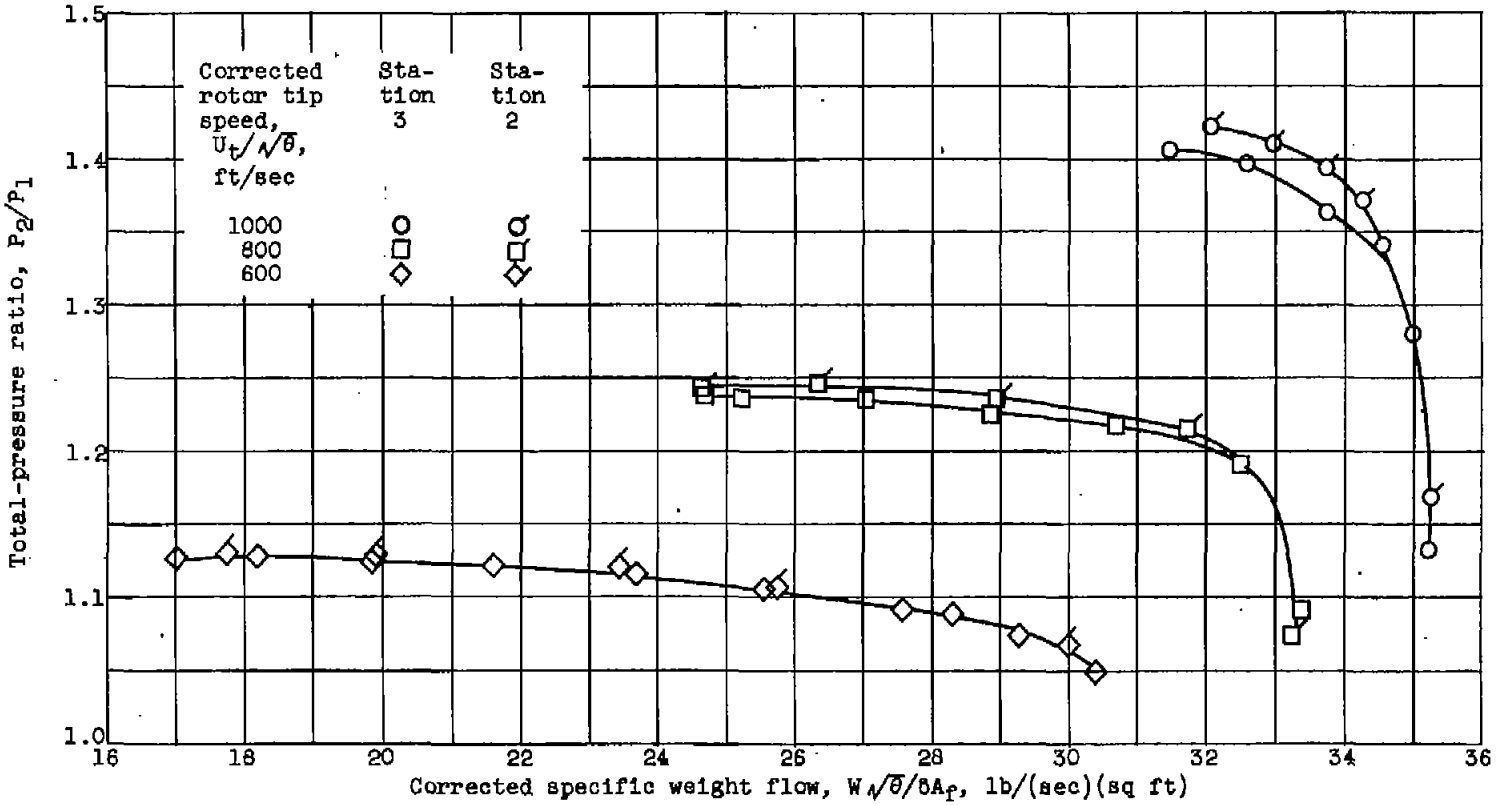

Figure 4. - Comparison of rotor-alone over-all performances as measured 1/2 inch (station 2) and 4 inches (station 3) downstream of blade trailing edge.

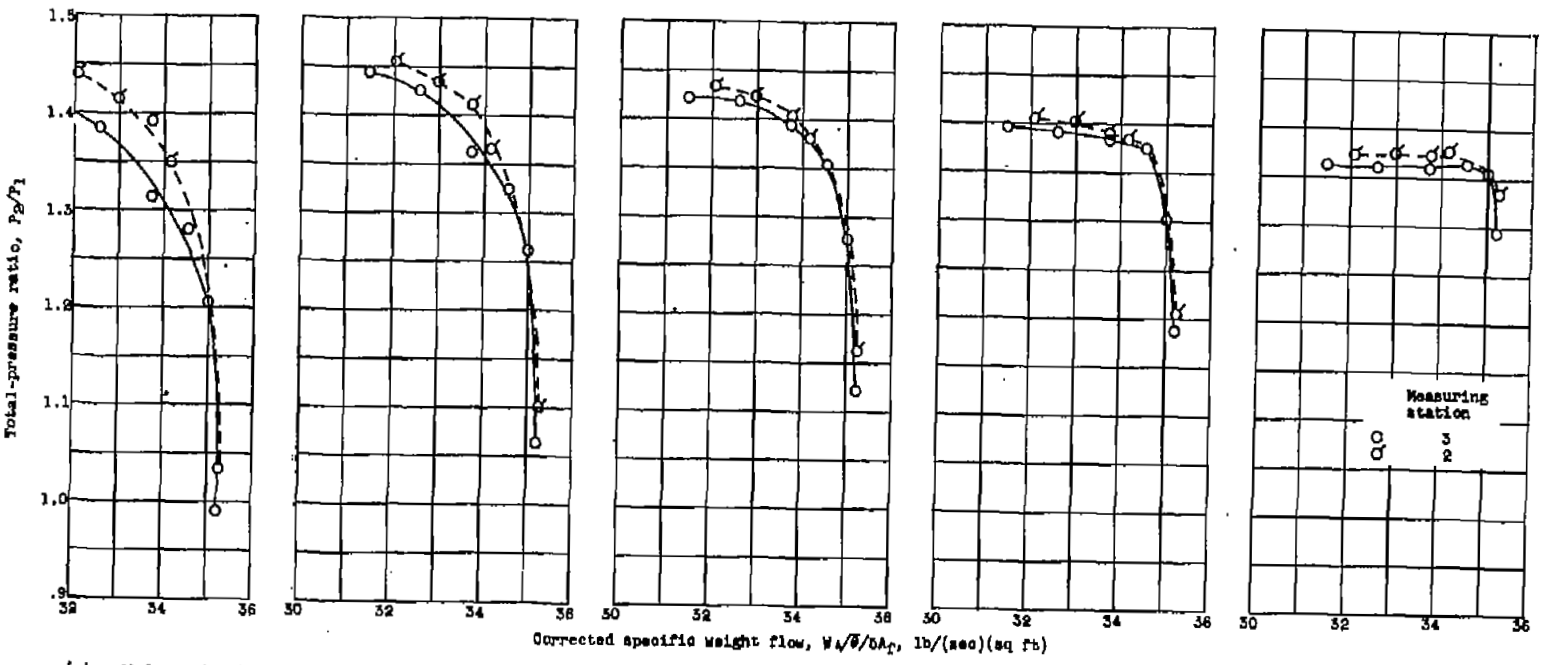

(a) Radial station A (near tip). (b) Radial station B. (c) Radial station C. (d) Radial station D. (e) Radial station E (near hub).

Figure 5. - Comparison of rotor-alone radial total-pressure ratio as measured 1/2 inch (station 2) and 4 inches (station 3) downstream of blade trailing edge. Corrected rotor tip speed $U_t/\sqrt{\theta}$, 1000 feet per second.

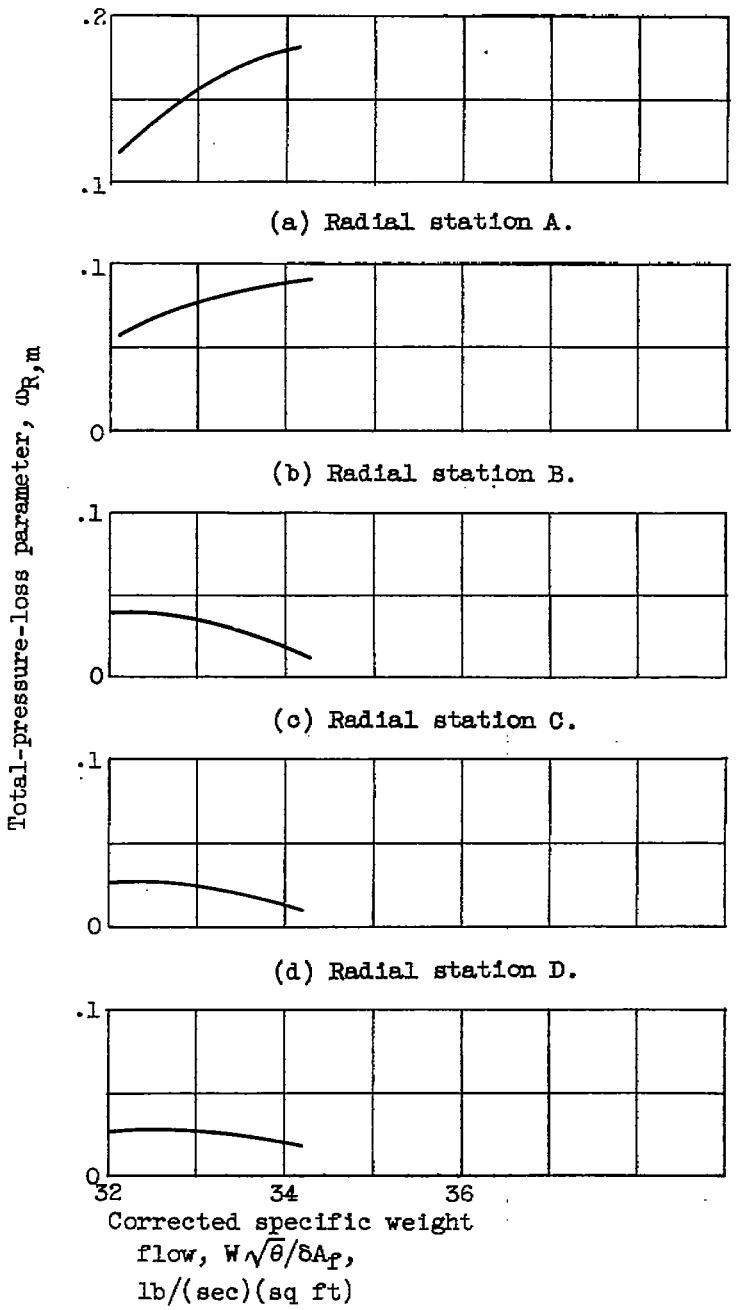

Figure 6. - Mixing-loss and probe-error total-pressure-loss coefficient for rotor. Design corrected tip speed $U_t/\sqrt{\theta}$, 1000 feet per second.

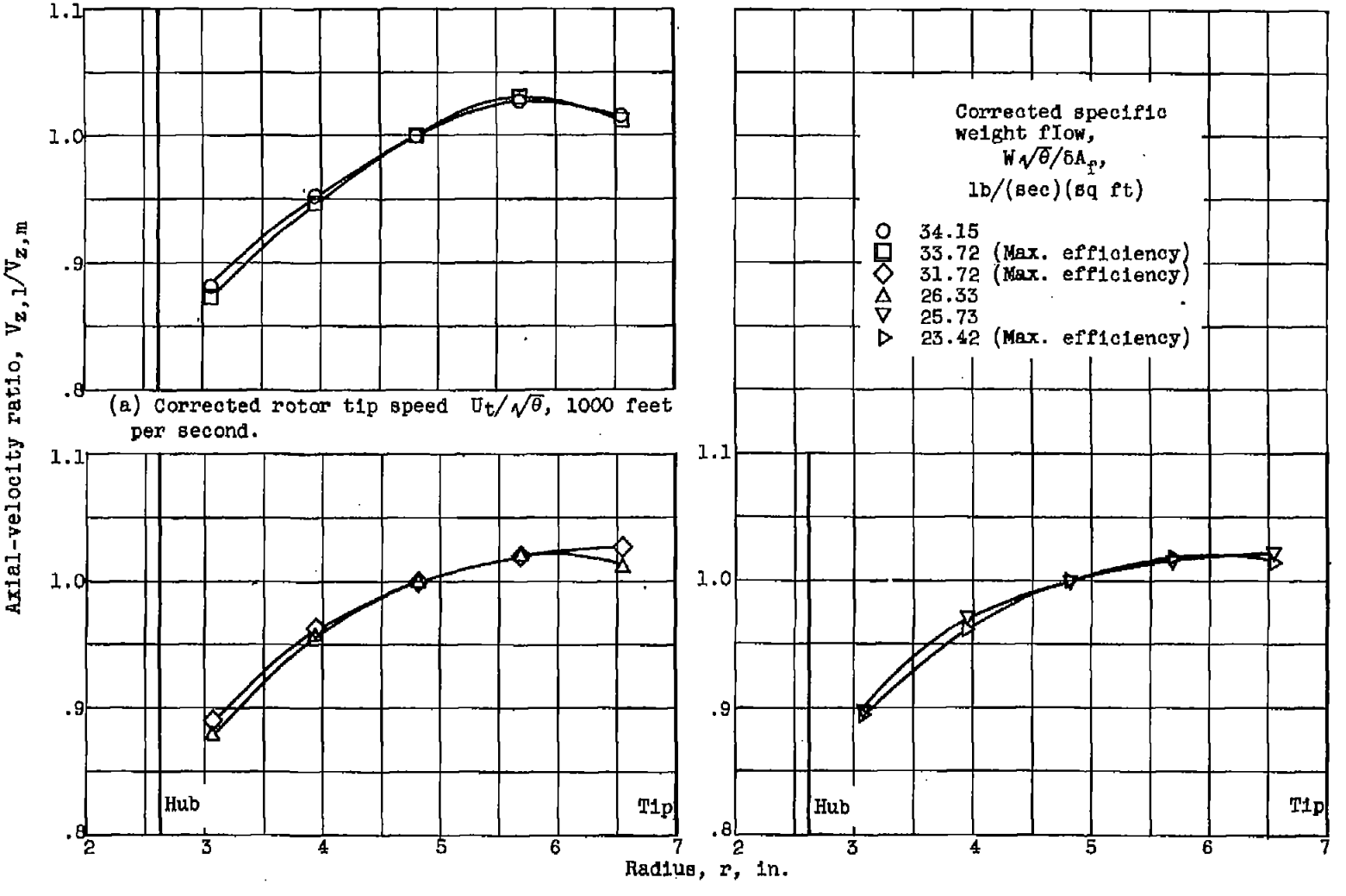

(a) Corrected rotor tip speed $U_t/\sqrt{\theta}$, 1000 feet per second.

(b) Corrected rotor tip speed $U_t/\sqrt{\theta}$, 800 feet per second.

(c) Corrected rotor tip speed $U_t/\sqrt{\theta}$, 600 feet per second.

Figure 7. - Variation of inlet axial-velocity ratio with radius at rotor inlet.

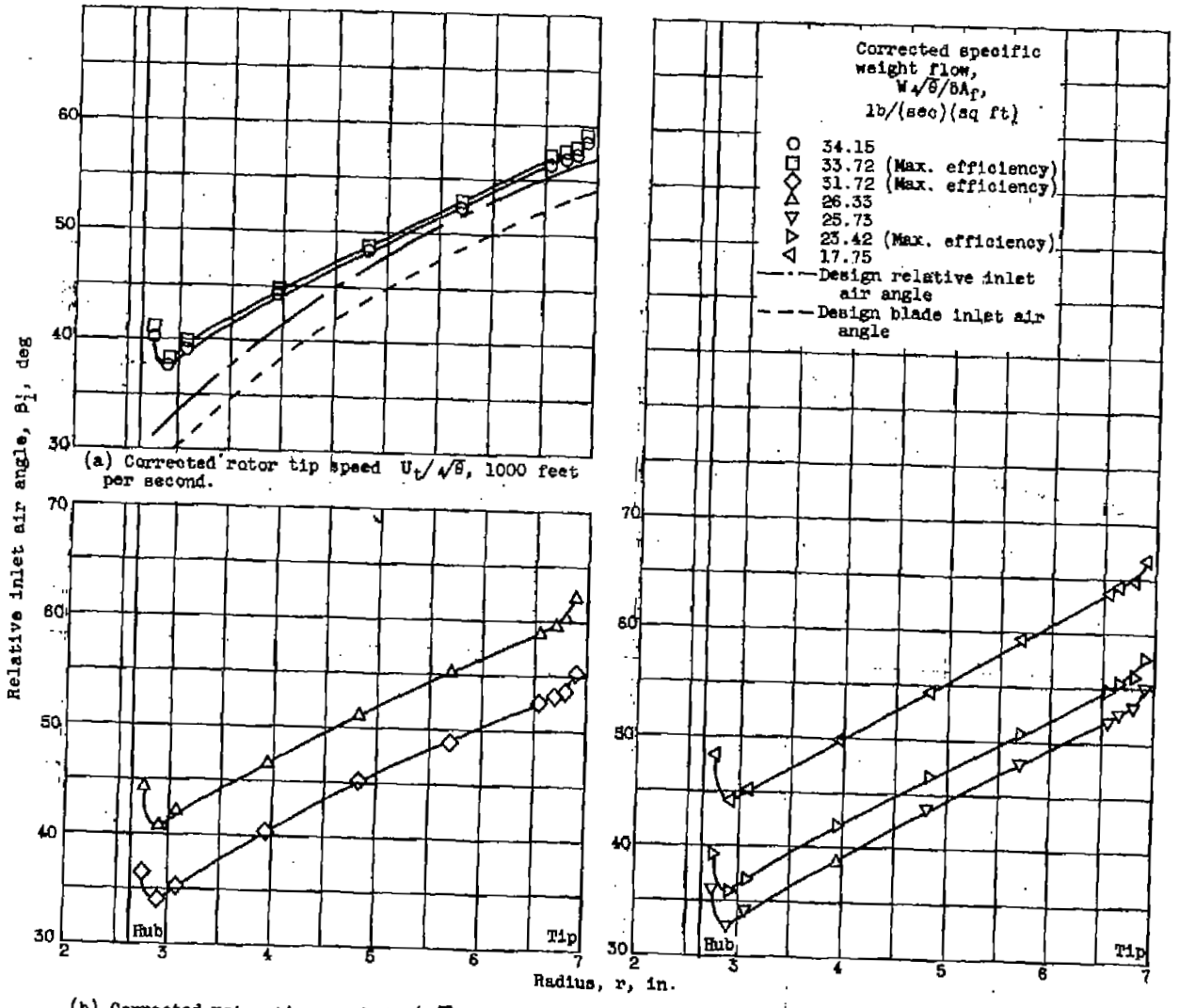

(a) Corrected rotor tip speed $U_t/\sqrt{\theta}$, 1000 feet per second.

(b) Corrected rotor tip speed $U_t/\sqrt{\theta}$, 800 feet per second.

(c) Corrected rotor tip speed $U_t/\sqrt{\theta}$, 600 feet per second.

Figure 8. - Variation of radial relative inlet air angle at rotor inlet.

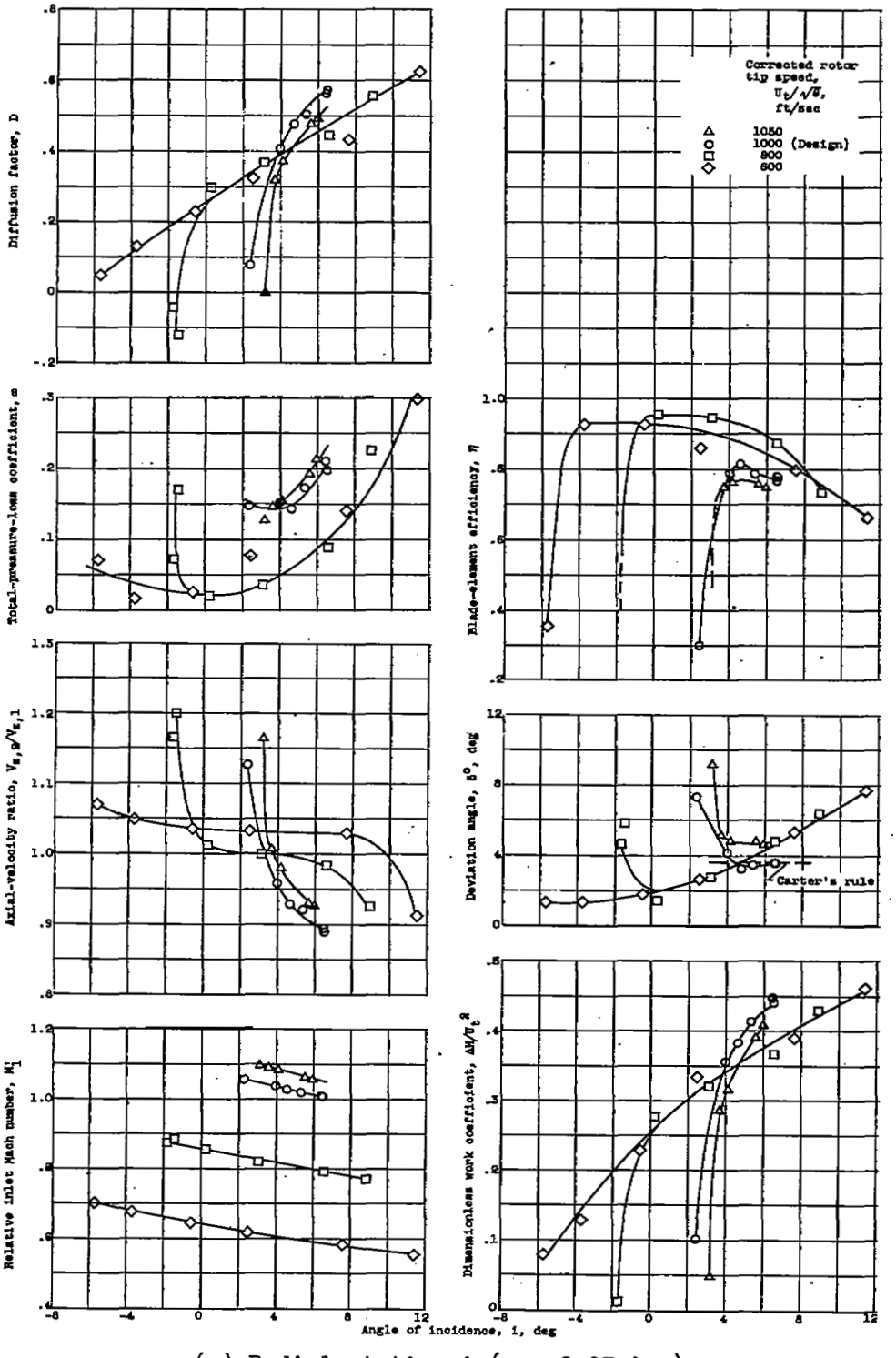

(a) Radial station A (r = 6.67 in.).

Figure 9. - Rotor-blade-element data.

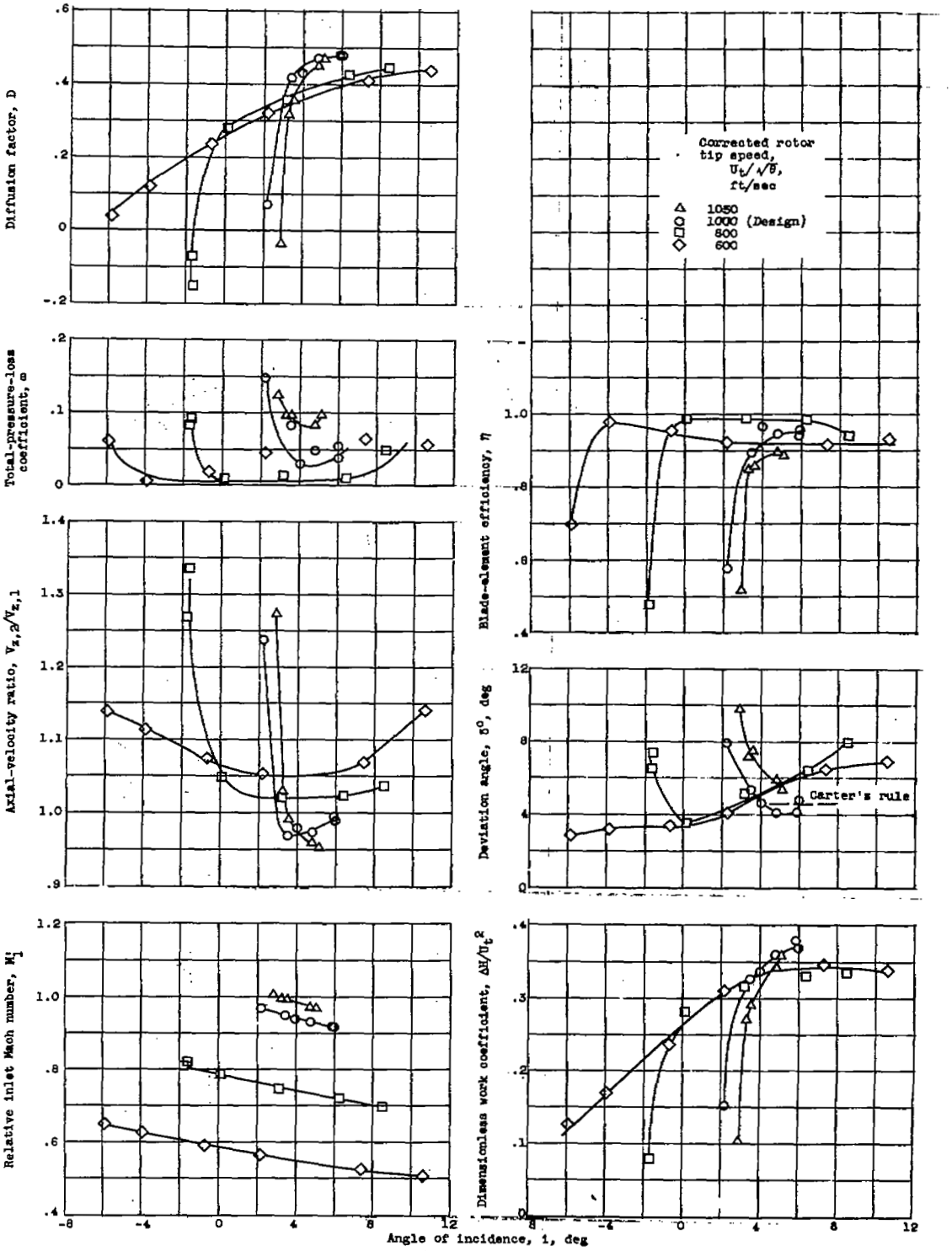

(b) Radial station B (r = 6.00 in.).

Figure 9. - Continued. Rotor-blade-element data.

[redacted]

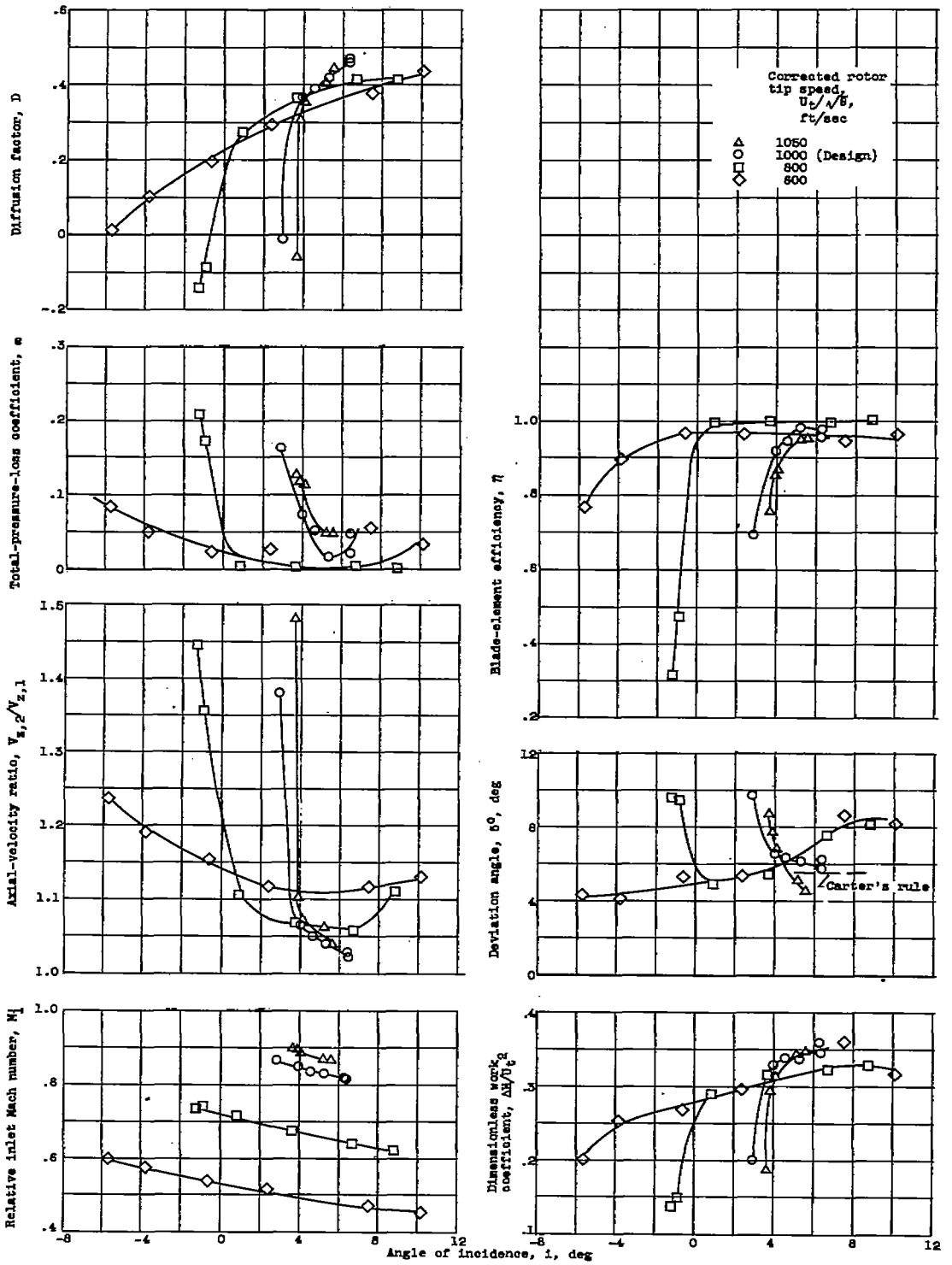

(c) Radial station C (r = 5.33 in.).

Figure 9. - Continued. Rotor-blade-element data.

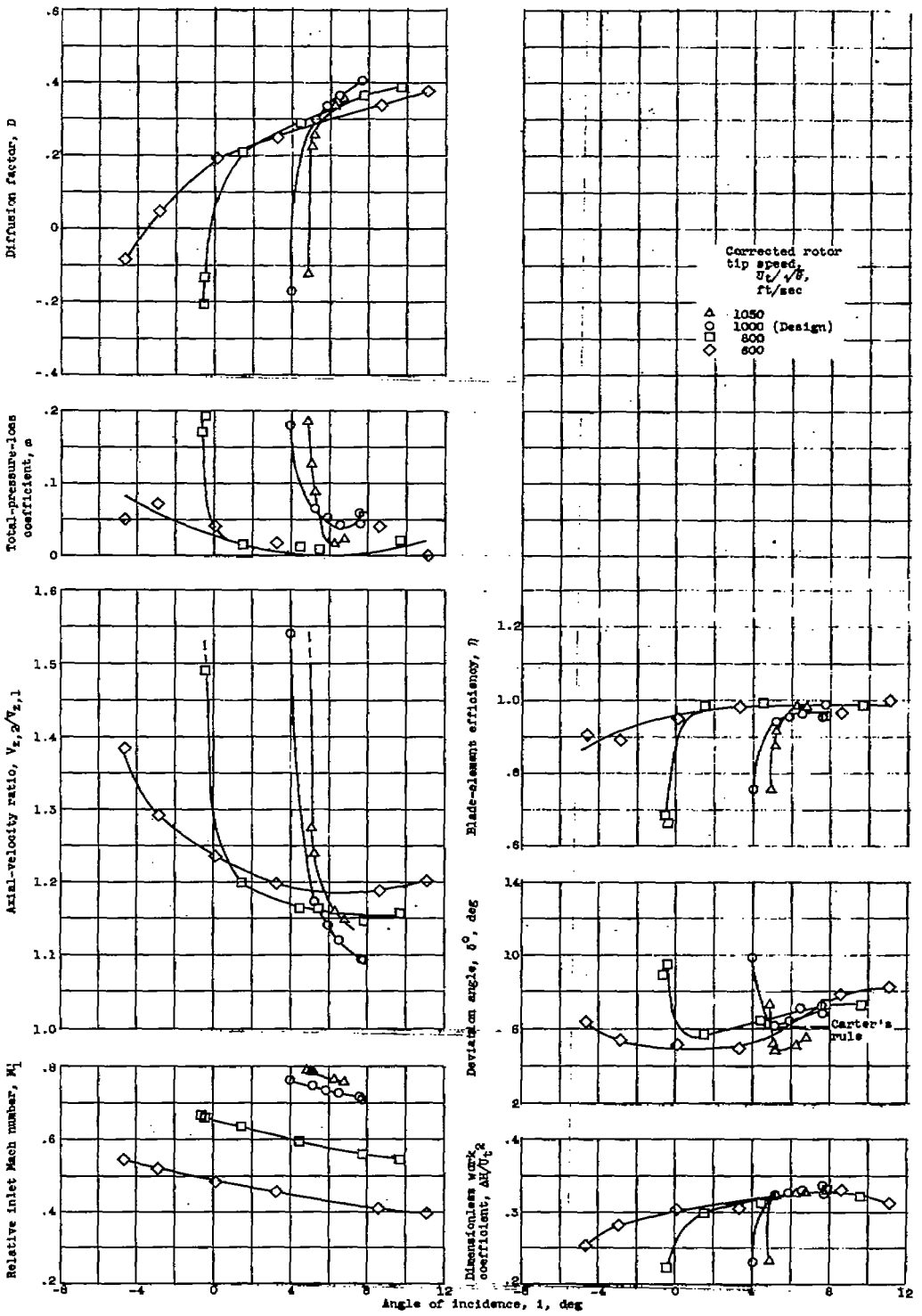

(d) Radial station D (r = 4.66 in.).

Figure 9. - Continued. Rotor-blade-element data.

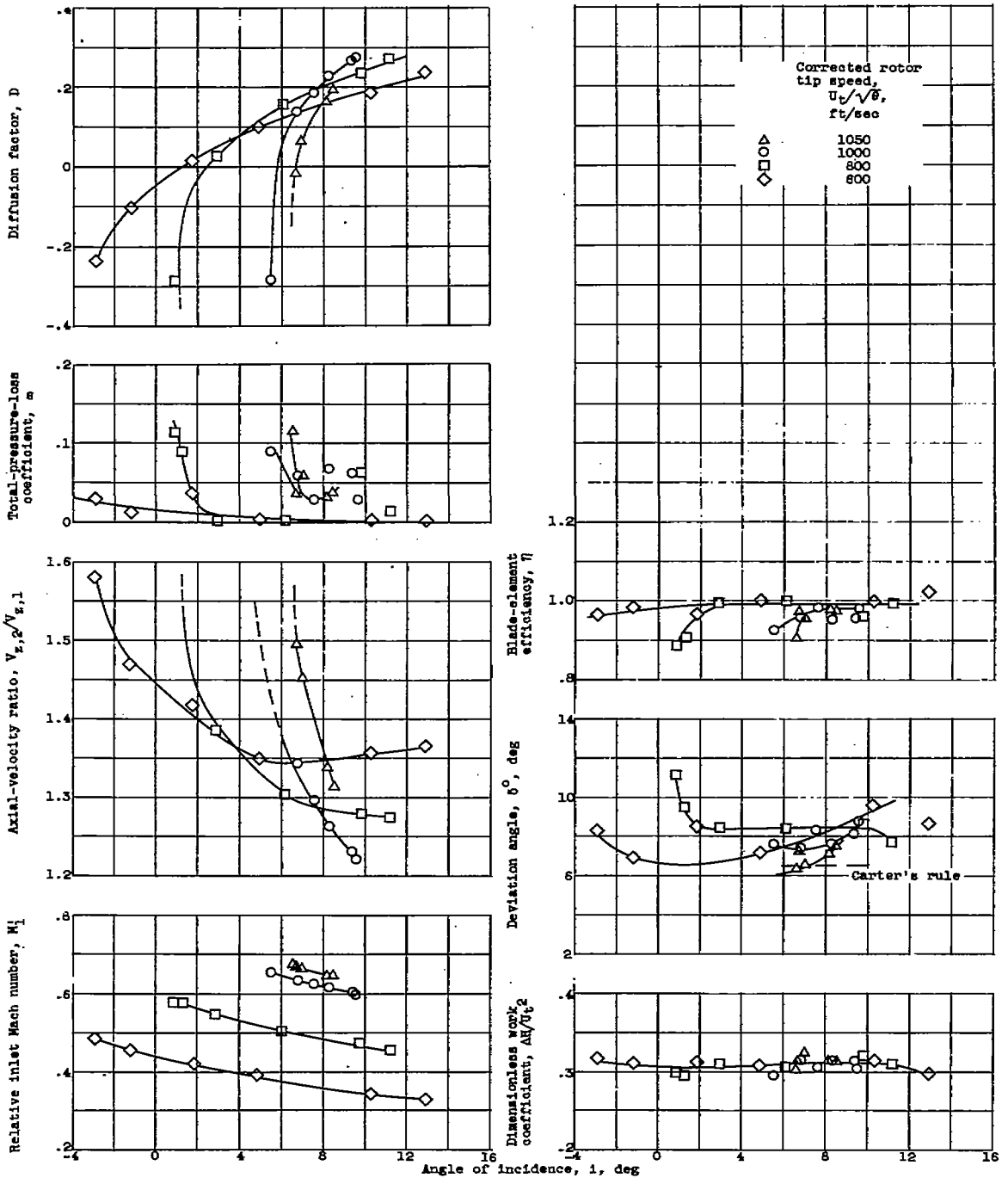

(e) Radial station E (r = 3.99 in.).

Figure 9. - Concluded. Rotor-blade-element data.

[redacted]

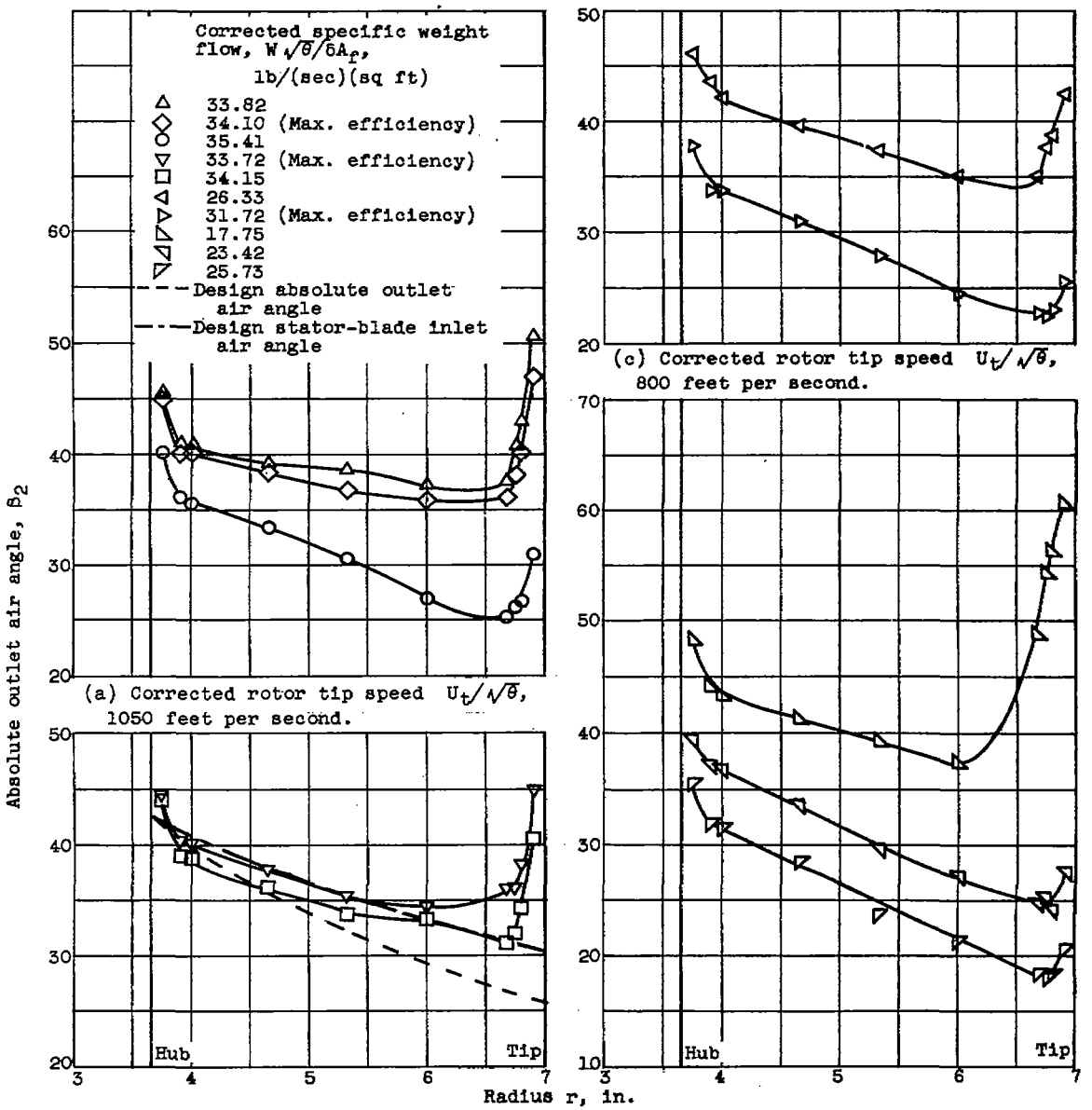

(a) Corrected rotor tip speed $U_t/\sqrt{\theta}$, 1050 feet per second.

(b) Corrected rotor tip speed $U_t/\sqrt{\theta}$, 1000 feet per second.

(c) Corrected rotor tip speed $U_t/\sqrt{\theta}$, 800 feet per second.

(d) Corrected rotor tip speed $U_t/\sqrt{\theta}$, 600 feet per second.

Figure 10. - Radial variation of absolute air angle at rotor outlet.

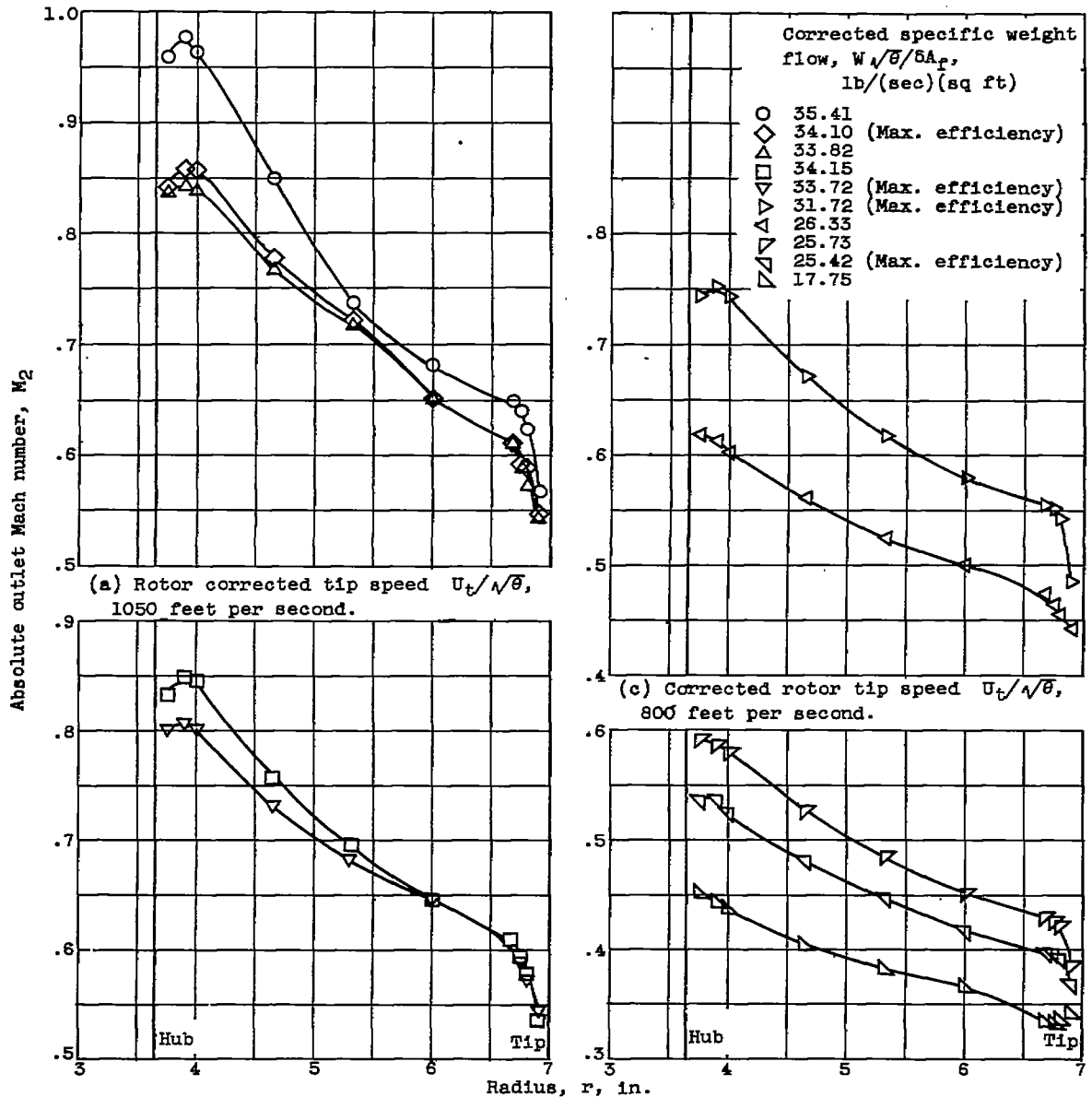

(a) Rotor corrected tip speed $U_t/\sqrt{\theta}$, 1050 feet per second.

(b) Corrected rotor tip speed $U_t/\sqrt{\theta}$, 1000 feet per second.

(c) Corrected rotor tip speed $U_t/\sqrt{\theta}$, 800 feet per second.

(d) Corrected rotor tip speed $U_t/\sqrt{\theta}$, 600 feet per second.

Figure 11. - Radial variation of absolute Mach number at rotor outlet.

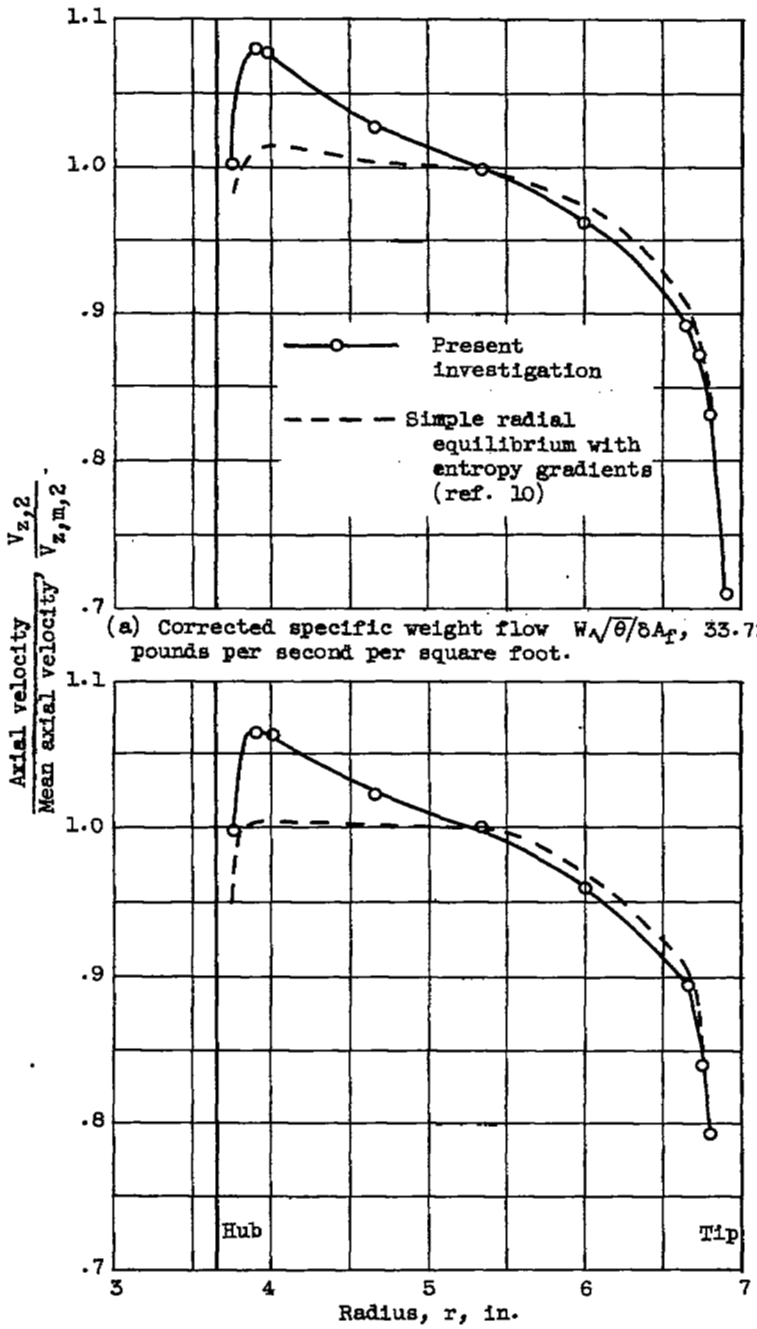

(a) Corrected specific weight flow $W\sqrt{\theta}/\delta A_f$, 33.72 pounds per second per square foot.

(b) Corrected specific weight flow $W\sqrt{\theta}/\delta A_f$, 32.96 pounds per second per square foot.

Figure 12. - Radial equilibrium comparison for rotor-outlet axial velocity. Rotor corrected tip speed $U_t/\sqrt{\theta}$, 1000 feet per second.

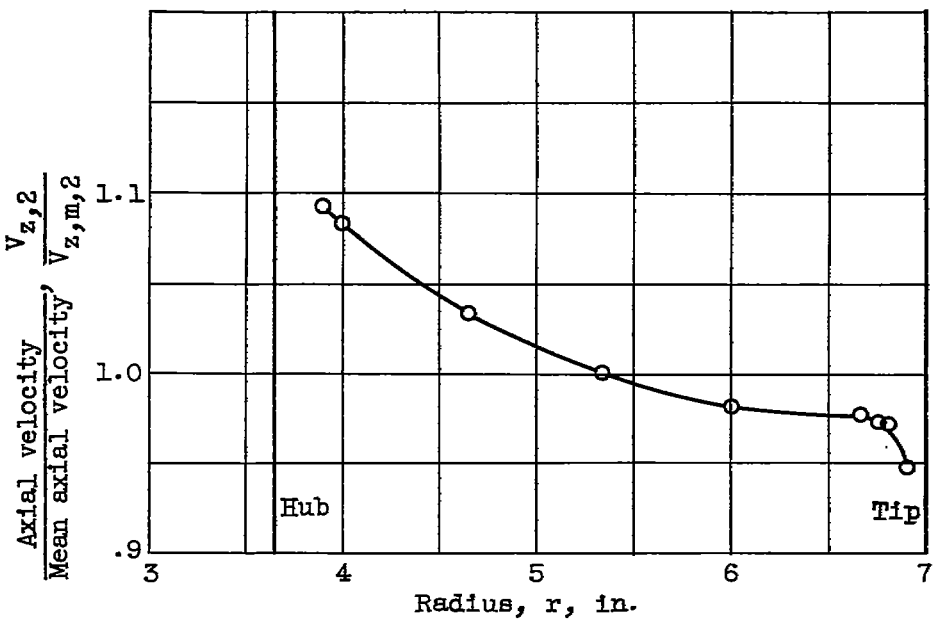

Figure 13. - Axial-velocity distribution at rotor outlet with rotor blades removed. Corrected specific weight flow $W\sqrt{\theta}/\delta A_f$, 32.68 pounds per second per square foot.

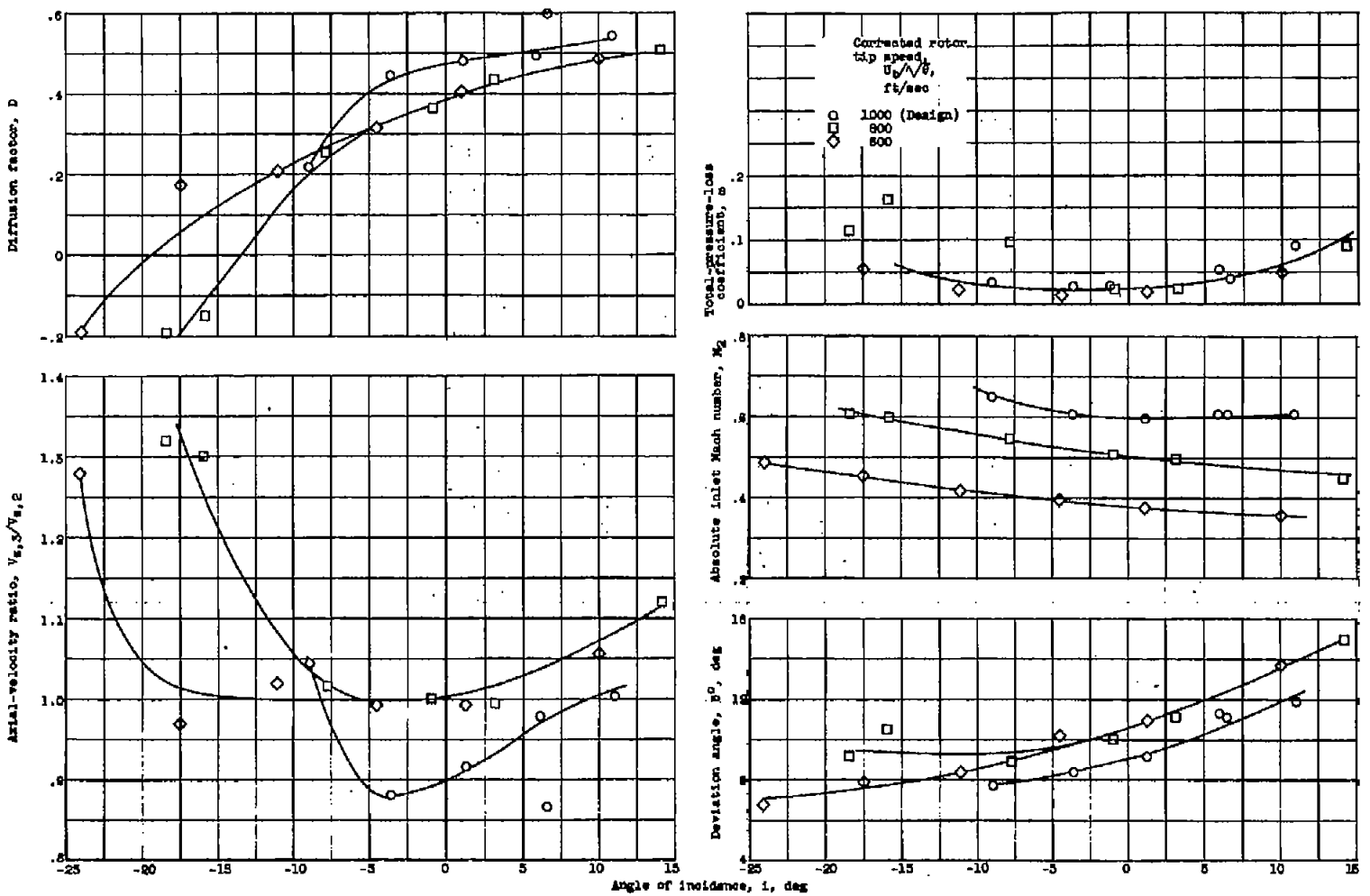

(a) Radial station A (r = 6.67 in.).

Figure 14. - Stator-blade-element data.

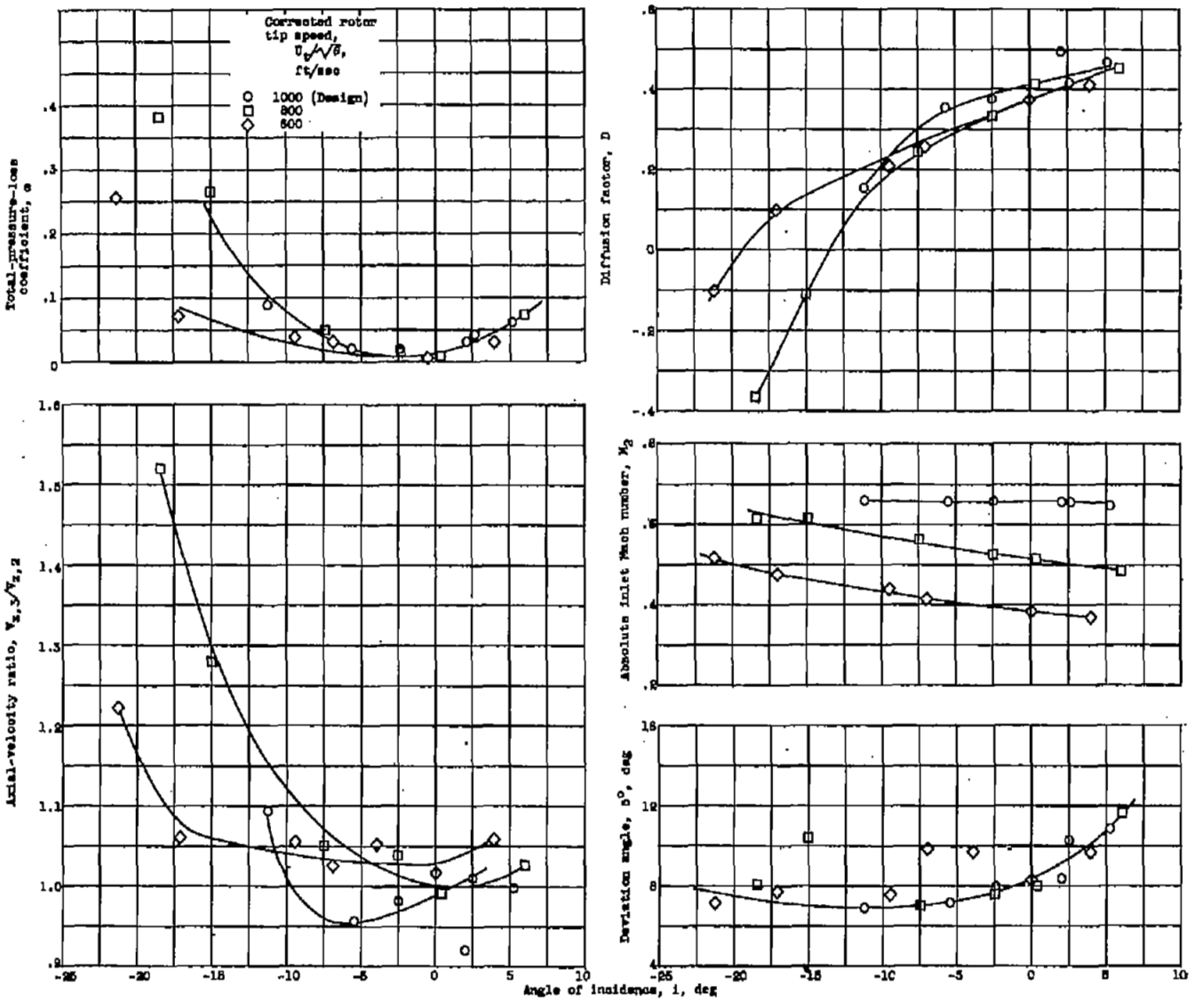

(b) Radial station B (r = 6.01 in.)

Figure 14. - Continued. Stator-blade-element data.

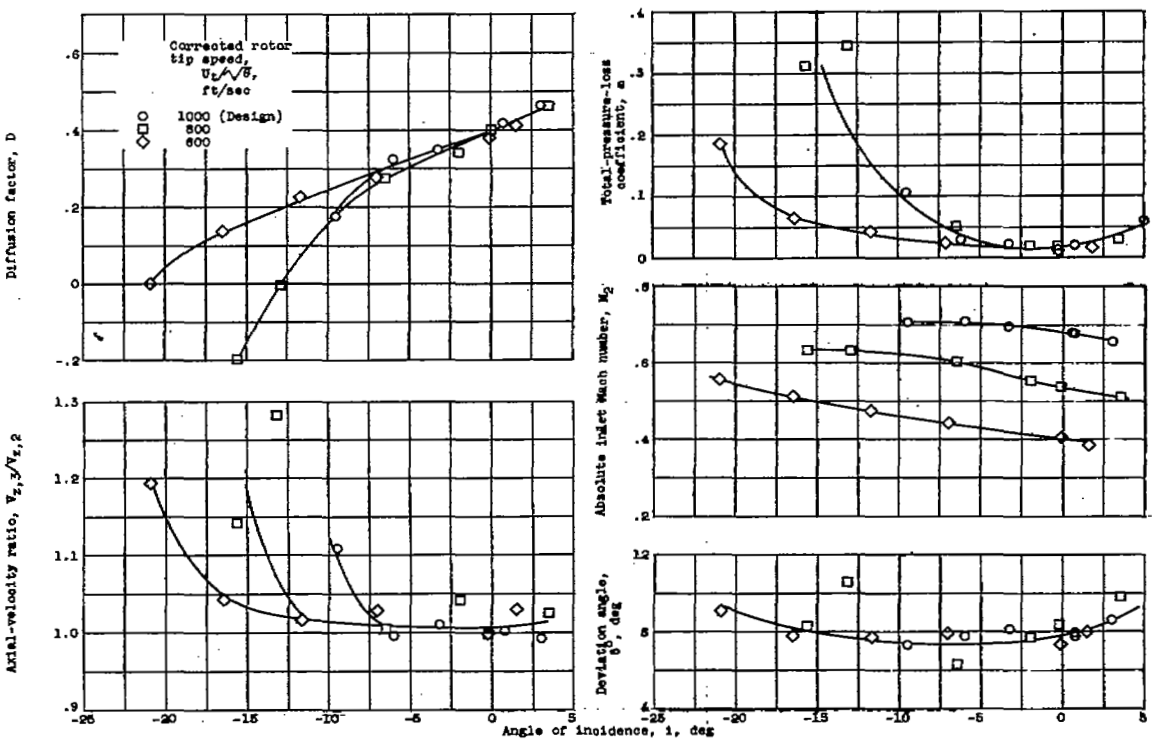

(c) Radial station C (r = 5.36 in.).

Figure 14. - Continued. Stator-blade-element data.

[redacted]

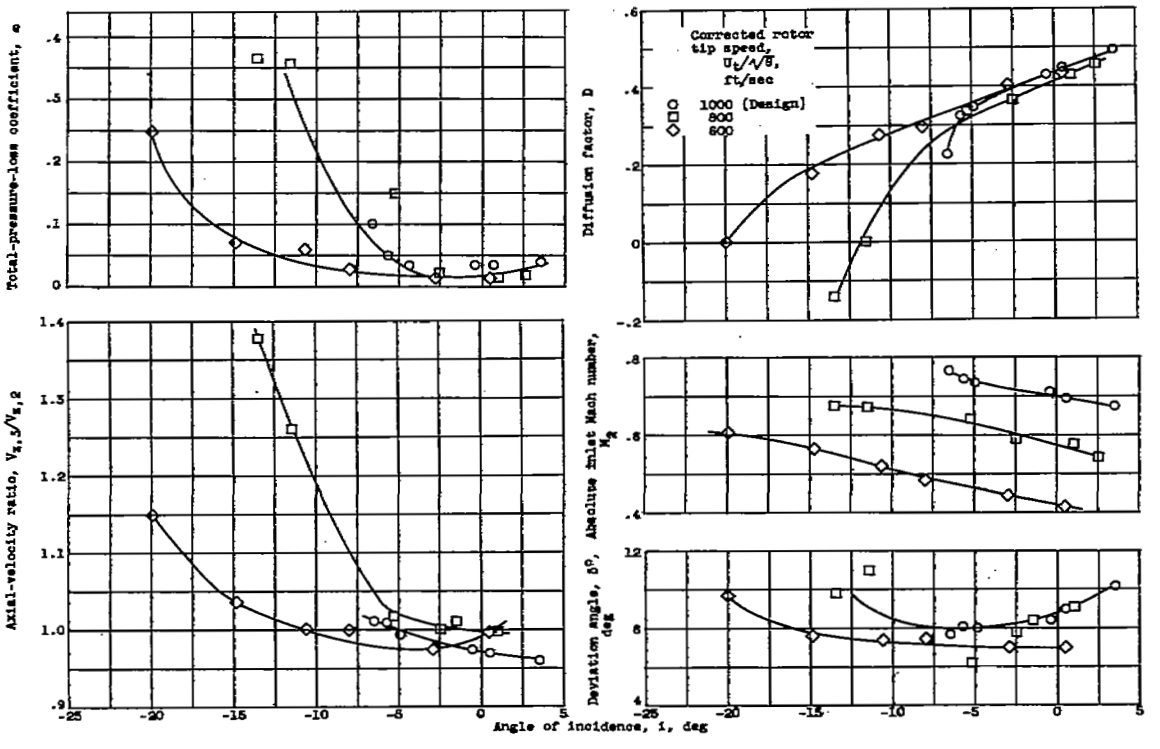

(d) Radial station D (r = 4.71 in.).

Figure 14. - Continued. Stator-blade-element data.

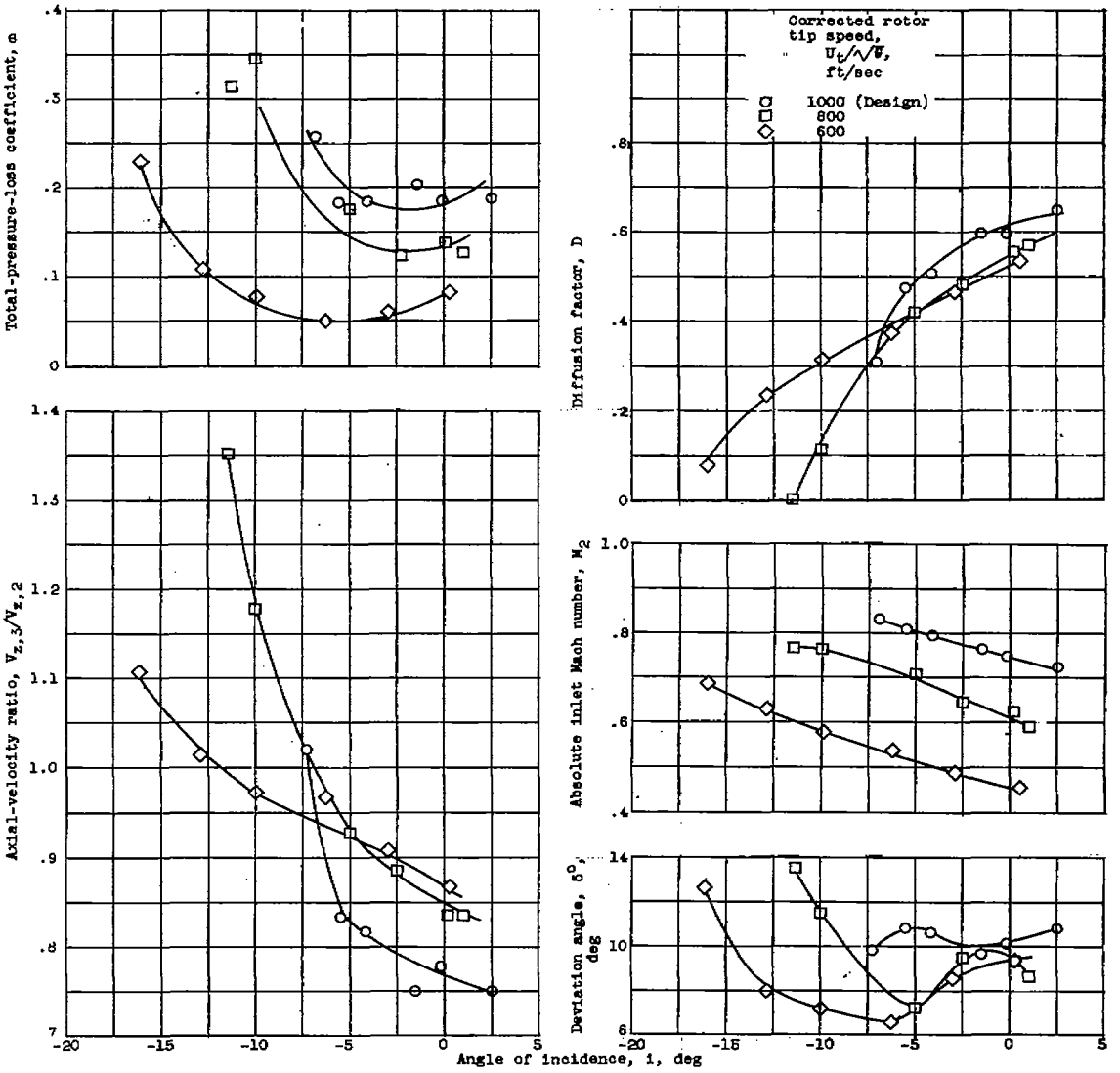

(e) Radial station E (r = 4.06 in.).

Figure 14. - Concluded. Stator-blade-element data.

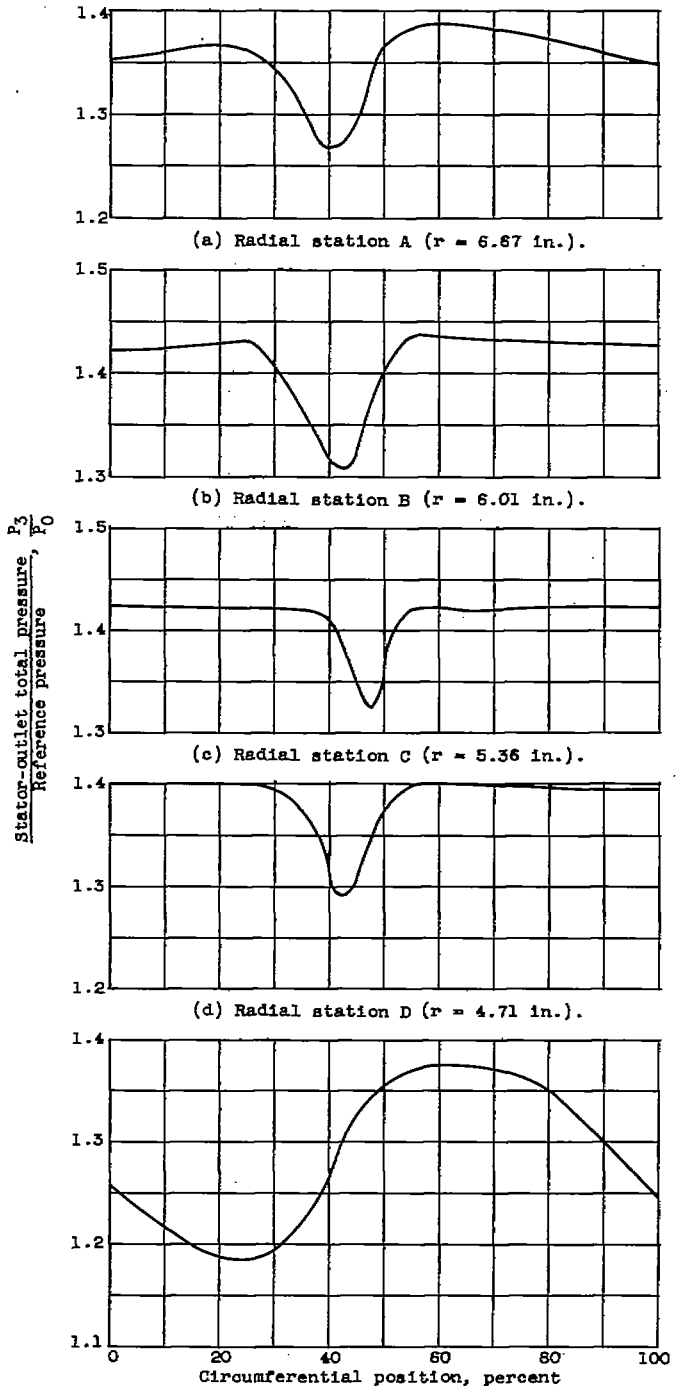

Figure 15. - Circumferential variation of measured total pressure at stator outlet. Corrected specific weight flow $W\sqrt{\theta}/\delta A_1$, 33.32 pounds per second per square foot; corrected rotor tip speed $U_t/\sqrt{\theta}$, 1000 feet per second.

[redacted]

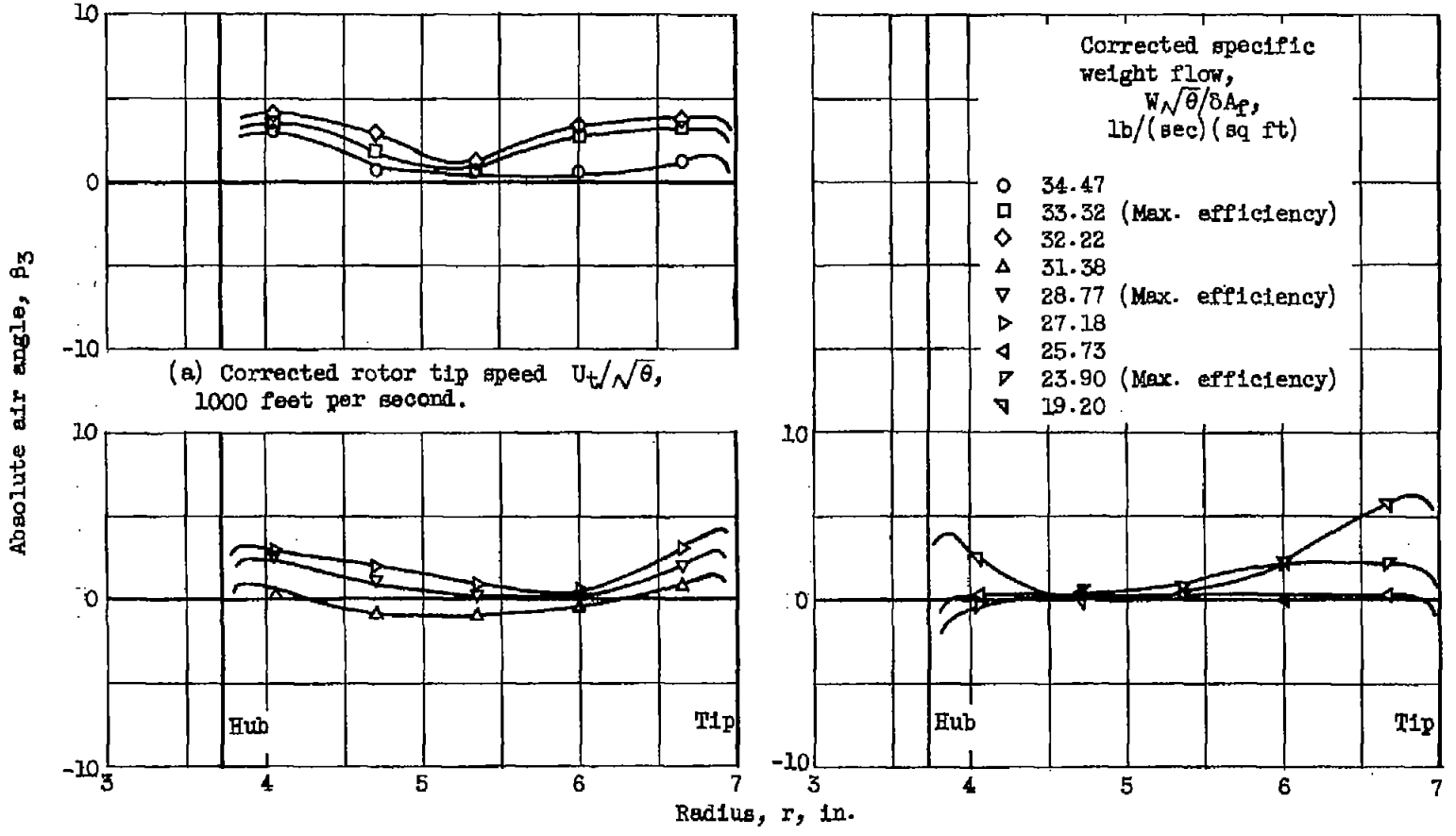

(a) Corrected rotor tip speed $U_t/\sqrt{\theta}$, 1000 feet per second.

(b) Corrected rotor tip speed $U_t/\sqrt{\theta}$, 800 feet per second.

(c) Corrected rotor tip speed $U_t/\sqrt{\theta}$, 600 feet per second.

Figure 16. - Radial variation of absolute air outlet angle at stator outlet.

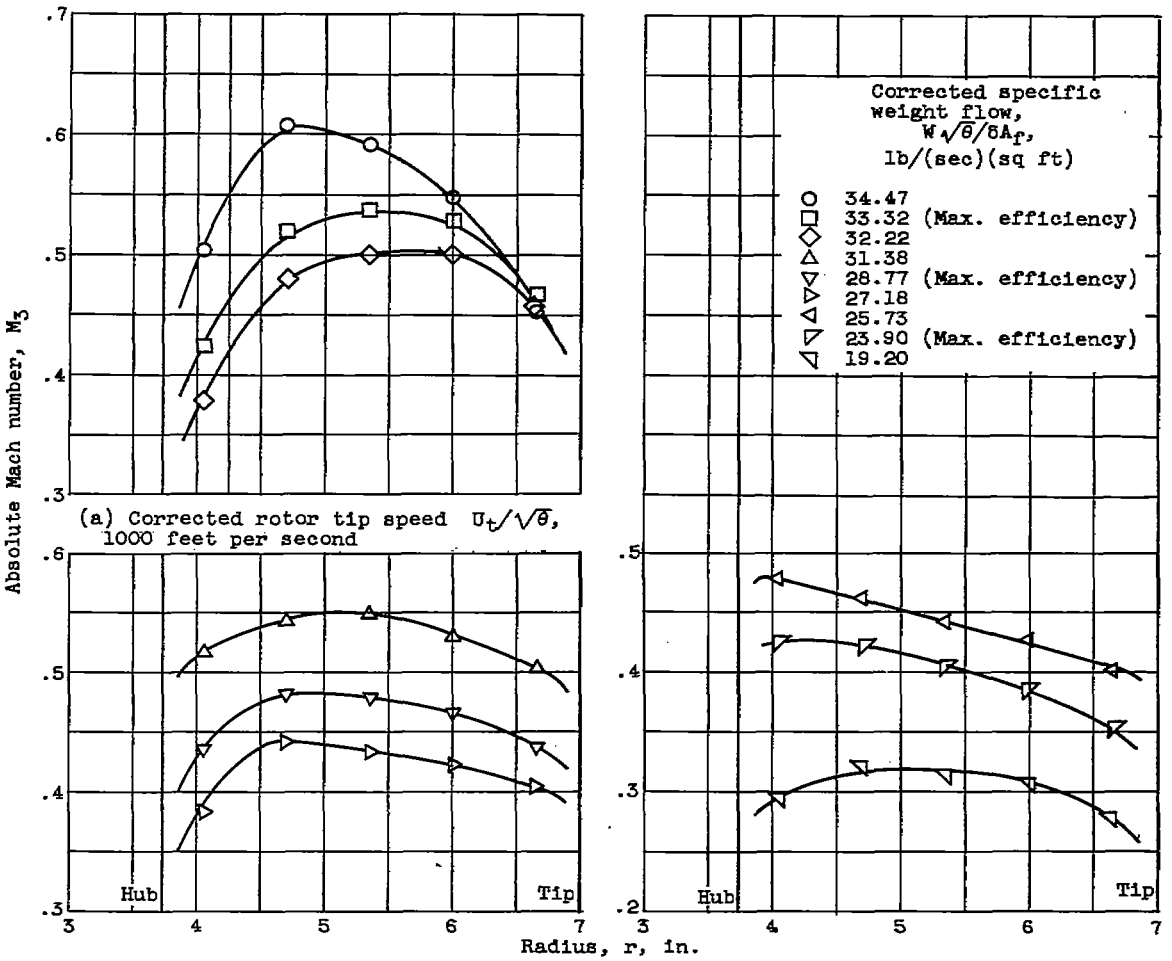

(a) Corrected rotor tip speed $U_t/\sqrt{\theta}$, 1000 feet per second

(b) Corrected rotor tip speed $U_t/\sqrt{\theta}$, 800 feet per second.

(c) Corrected rotor tip speed $U_t/\sqrt{\theta}$, 600 feet per second.

Figure 17. - Radial variation of absolute Mach number at stator outlet.

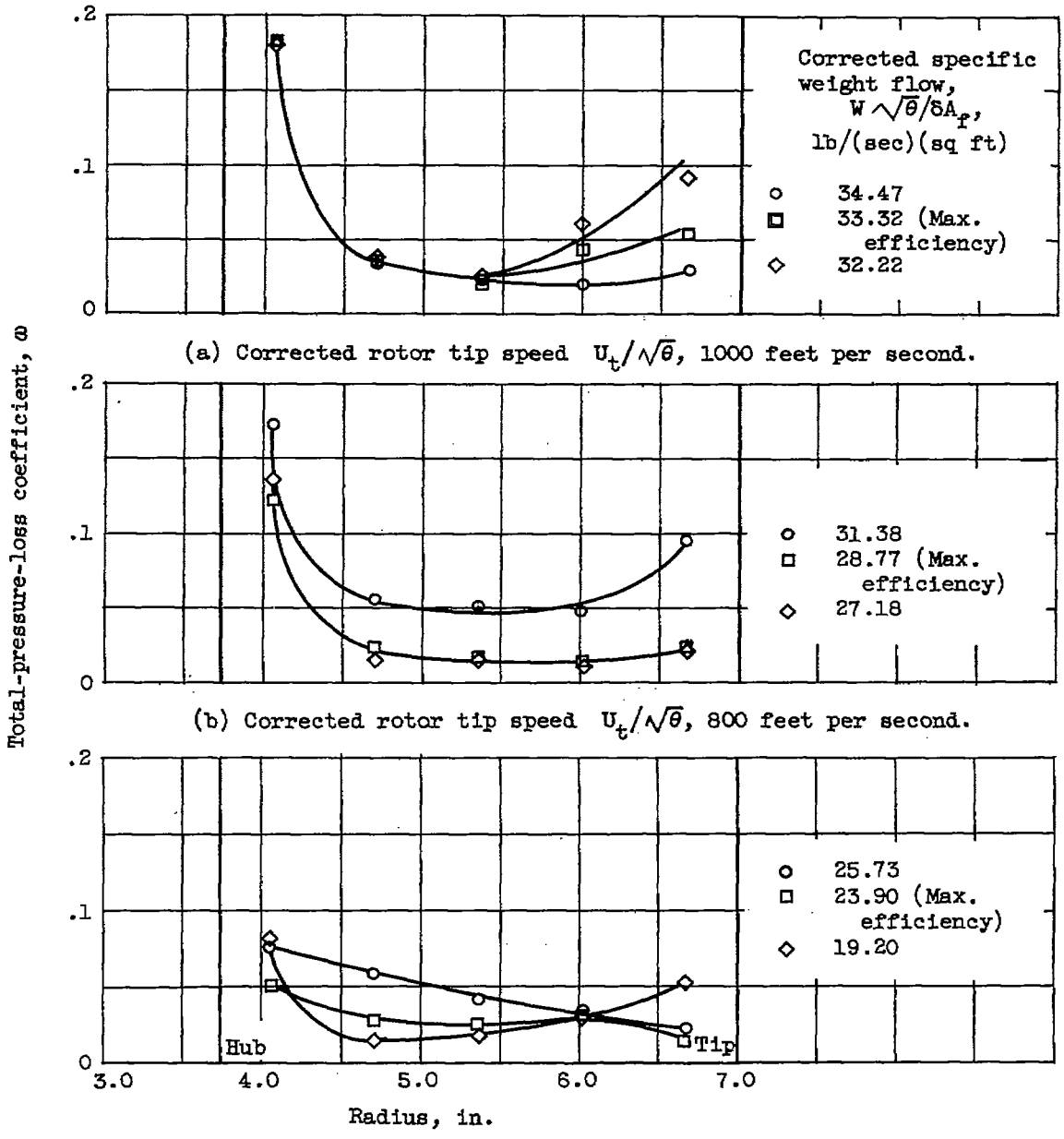

(a) Corrected rotor tip speed $U_t/\sqrt{\theta}$, 1000 feet per second.

(b) Corrected rotor tip speed $U_t/\sqrt{\theta}$, 800 feet per second.

(c) Corrected rotor tip speed $U_t/\sqrt{\theta}$, 600 feet per second.

Figure 18. - Radial variation of total-pressure-loss coefficient at stator outlet.

NACA-Langley - 1-10-55 - 350